

# Coded Hierarchical Modulation for Wireless Progressive Image Transmission

Suayb S. Arslan, *Student Member, IEEE*, Pamela C. Cosman, *Fellow, IEEE*, and Laurence B. Milstein, *Fellow, IEEE*

**Abstract**—A robust coded scheme for progressive multimedia transmission is proposed for additive white Gaussian noise, flat Rayleigh fading channels, and frequency-selective channels using different unequal error protection methods in combination. Hierarchical modulation is coupled with a packetization/combining strategy and an efficient channel encoder consisting of a cyclic redundancy check outer coder concatenated with an inner rate-compatible punctured convolutional coder. Distortion-optimal hierarchical parameters are jointly chosen with the set of channel coding parameters on a packet-switched wireless network with fixed length packets. A lower bound for the performance improvement of the proposed system is derived and shown to give significant gains at lower packet sizes and higher transmission rates. The proposed system is also shown to outperform several existing schemes for realistic wireless channels.

**Index Terms**—Hierarchical modulation, image coding, joint source channel coding (JSCC), link breakage, packetization, progressive source transmission, unequal error protection (UEP).

## I. INTRODUCTION

IN PROGRESSIVE bit streams, the significance of bits decreases with each successive bit. Due to the embedded coding structure, compressed data exhibit different error sensitivities in different parts of the progressive bit stream and are often very vulnerable to channel errors. Forward error correction (FEC) can be used to address this problem in the absence of feedback with lower code rates for the beginning of the stream and higher rates later on to provide unequal error protection (UEP) to the bits of unequal importance. This is usually called joint source channel coding (JSCC). JSCC-only mechanisms are extensively considered in the literature for progressive coding. In [1] and [2], UEP is provided with nonuniform channel codes for different parts of the encoded image. In [3]–[5], rate compatible punctured convolutional (RCPC) channel codes, turbo codes, and low-density parity check (LDPC) codes are applied to source packets to improve the performance of

memoryless channels. RCPC codes are also considered in [6] by applying different channel code rates for different kinds of bits (e.g., sign bits, wavelet coefficient bits, etc.) of set-partitioning-in-hierarchical-trees (SPIHT) [7] encoded data. However, those studies consider simple channel models such as binary symmetric channels (BSCs) or additive white Gaussian noise (AWGN) with a binary alphabet. Studies such as [8] divide the UEP task between both the channel encoder and the modulator to help reduce the convolutional coding complexity and provide unequal protection using a single code rate for the transmission. More recently, studies such as [9] considered modulation-assisted UEP-LDPC codes to achieve a good tradeoff between reliability and spectrum efficiency using a three-level LDPC code and a quadrature phase-shift keying/16 quadrature amplitude modulation (QAM) mapping for UEP. In addition, JSCC is considered in an orthogonal frequency-division-multiplexing setting in [10] to combat intersymbol interference (ISI) and is combined with space time codes in [11] to provide diversity gains.

Hierarchical modulation is yet another popular strategy to provide UEP. It has been included in various standards [12] and used to give unequal transmission reliability to high priority (HP) and low priority (LP) bits [13]–[15]. Fig. 1 illustrates several hierarchical constellations, where the hierarchical parameter  $\alpha$  adjusts the distances of the symbol points in the constellation. As shown in Fig. 1,  $\alpha$  is the ratio of the distances of the symbols to the origin on one side of the constellation. In going from one constellation to another, we change  $\alpha$  so that HP bits and LP bits will have different error probabilities. Hierarchical 16-QAM (H-16QAM) and hierarchical 64-QAM (H-64QAM) are simple extensions to H-4PAM and H-8PAM, respectively, by considering in-phase and quadrature components as two independent constellations. We usually constrain the average bit energy  $E_b$  to be the same for any  $\alpha$ . The idea of hierarchical modulation combined with progressively compressed signals is not new. In [14], the authors consider hierarchical modulation and progressive image layers encoded using an adaptive discrete cosine transform. Hierarchical modulation is used without channel coding in wireless relay networks in [16] and is shown to yield good unequal protection capability. Adaptive modulation is considered in [17] and [18] within the framework of JSCC. In addition, [19] considers both hierarchical modulation and channel coding to provide UEP for two-layer video transmission. The unequal protection is achieved by one of the UEP mechanisms while respecting the delay limitations of the transferred video. To the best of our knowledge,

Manuscript received January 5, 2011; revised April 16, 2011 and July 16, 2011; accepted July 18, 2011. Date of publication July 29, 2011; date of current version December 9, 2011. This work was supported in part by LG Electronics Inc., by Intel Inc., by the Center for Wireless Communications at the University of California at San Diego, by the University of California Discovery Grant Program of the state of California, and by the National Science Foundation under Grant CCF-0915727. This paper was presented in part at the IEEE Global Communications Conference, Honolulu, HI, December 2009. The review of this paper was coordinated by Dr. K. T. T. Wong.

The authors are with the Department of Electrical and Computer Engineering, University of California, San Diego, La Jolla, CA 92093-0407 USA (e-mail: sarslan@ucsd.edu; pcosman@ucsd.edu; lmilstein@ucsd.edu).

Color versions of one or more of the figures in this paper are available online at <http://ieeexplore.ieee.org>.

Digital Object Identifier 10.1109/TVT.2011.2163179

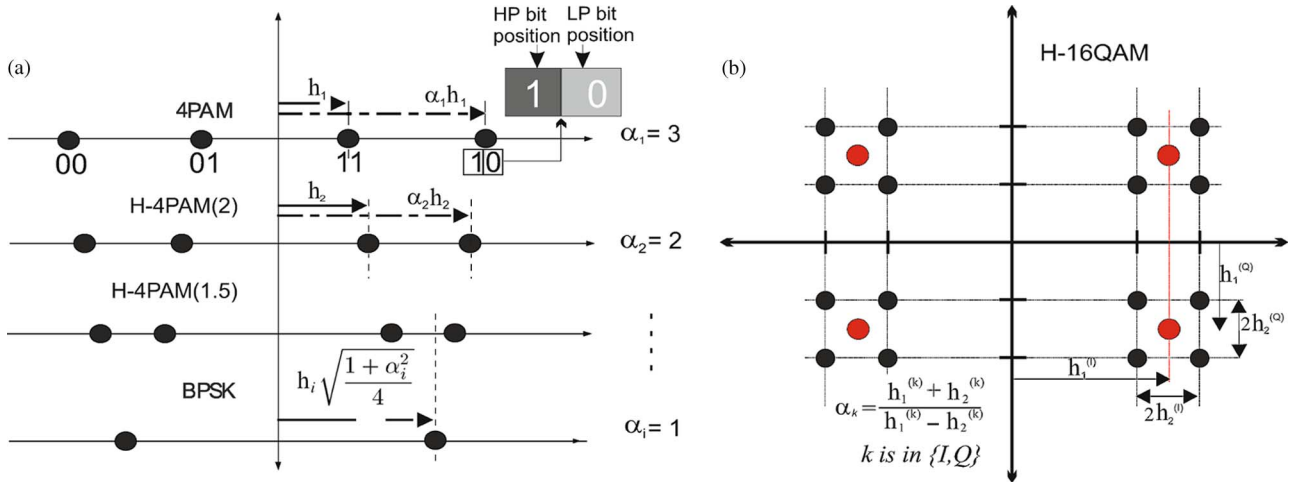


Fig. 1. Hierarchical modulation. (a) 4PAM ( $\alpha_1 = 3$ , top), H-4PAM [ $\alpha_2 = 2$ ,  $\alpha = 1.5$ , middle two], and binary phase-shift keying to which it collapses when  $\alpha_i = 1$  (bottom). (b) Hierarchical 16QAM (H-16QAM) can be considered as two independent H-4PAM signaling as the in-phase and quadrature components of the original constellation. We keep  $E_b$  constant across all constellations.

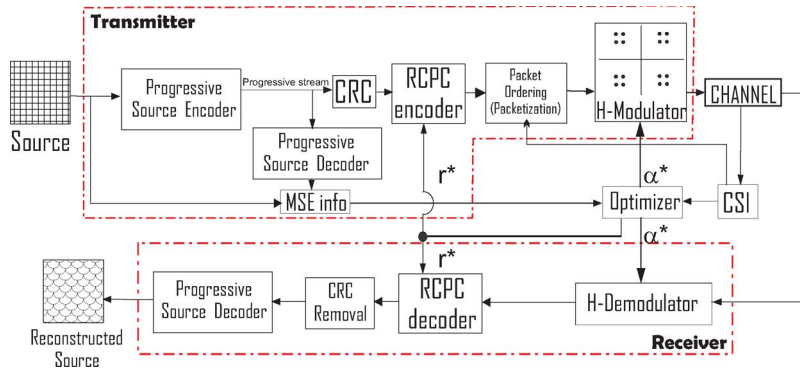


Fig. 2. Baseline system model with related block diagrams. Explanation for each block is given in the text. System is adaptive according to channel conditions.

the proposed work is the first study that combines hierarchical modulation, JSCC and packetization together in a distortion optimal way and addresses their interaction in a progressive transmission scenario.

A problem with JSCC is that adding more redundancy constrains the available bandwidth for the source bits. In contrast, hierarchical modulation can provide UEP without constraining the bandwidth. Although progressive multimedia sources can be protected using each method separately, in this study, we will show combining channel coding with hierarchical modulation can take advantage of both. We consider RCPC codes, but the proposed methodologies can be applied to more powerful codes, such as turbo and LDPC codes, for improved performance using iterative decoding algorithms, at the expense of complexity. We finally note that some of the gains reported in [4] and [5] compared with [2] and [6] can be attributed to the superiority of capacity-achieving codes over conventional coding schemes rather than strictly attributing the gains to the manner in which the FEC is deployed.

The main contribution of this study is to address how to combine different UEP mechanisms effectively in a progressive transmission scenario for different wireless channel models for a given bandwidth constraint. A novel packetization strategy is introduced to combine encoded packets of different importance levels through hierarchical modulation to provide a

more flexible system than existing coded transmission schemes. We consider a single-carrier system to transmit fixed-length packets (but variable payload size within the packet). We initially consider AWGN and slowly varying flat Rayleigh fading channels and then extend some of the simulation results to frequency-selective channels with equalization. We show that different UEP methods can be combined to provide enhanced progressive source transmission using efficient combining strategies.

The remainder of this paper is organized as follows: In Section II, the system model is described in detail. In Section III, different bit-to-symbol assignment strategies are summarized. In Section IV, hard decision upper bounds for coded hierarchical modulation are given, and the optimization problem is constructed and solved. A lower bound is derived for the performance improvement of the proposed system. Some of the performance results for memoryless channels are given at the end of the section. Section V discusses a frequency-selective channel that models a link breakage scenario and introduces ISI. Finally, conclusions follow in Section VI.

## II. SYSTEM MODEL

A block diagram of the progressive transmission system is shown in Fig. 2. A progressive source encoder produces the

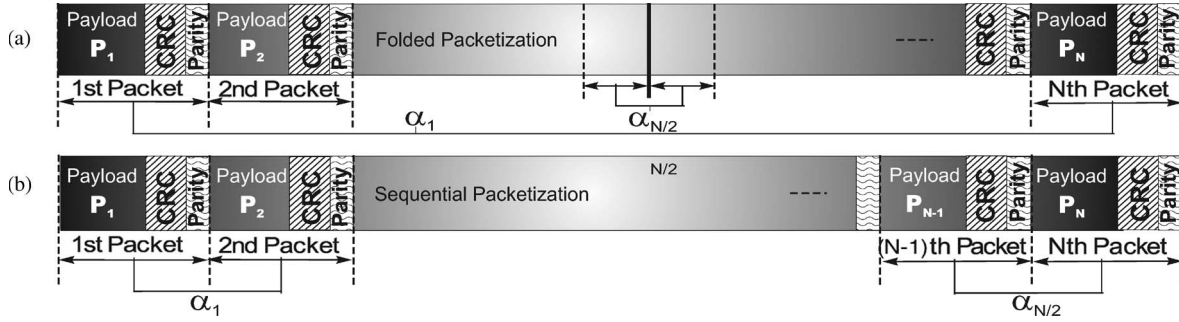


Fig. 3. Two different assignments of packetized bits to symbols (out of  $\prod_{i=1}^{(N/2)-1} \binom{N-2i}{2}$  different possible ways) in a progressively encoded source.  $P_i$ :  $i$ th chunk of information. Although CRC and parity blocks of bits are shown to be of equal size, the optimization can allocate different numbers of information and parity bits for each packet.

bit stream. A decoder implemented at the encoder reconstructs the compressed source and extracts the rate–distortion characteristics. The distortion  $d_l$  that results upon receiving packets up to and including packet  $l$  is determined. We use mean square error (MSE) as our distortion metric. The physical meaning of MSE is the cumulative squared error between the reconstructed image at the receiver and the original image. In particular,  $d_l$  is given by

$$d_l = \frac{1}{L_x L_y} \sum_{k=1}^{L_x} \sum_{s=1}^{L_y} |I(k, s) - R_l(k, s)|^2. \quad (1)$$

where  $L_x$  and  $L_y$  are the horizontal and vertical sizes of the image in pixels,  $I(k, s)$  is the original image pixel value at  $(k, s)$ , and  $R_l(k, s)$  represents the reconstructed image pixel value using only the first  $l$  packets of the encoded packet stream.

We denote the set of bits that are in the  $l$ th packet  $\mathcal{P}_l$  and the sets of bits in the first and second halves of the packet stream  $\mathcal{P}'_{\cup} = \bigcup_{l=1}^{N/2} \mathcal{P}_l$  and  $\mathcal{P}''_{\cup} = \bigcup_{l=(N/2)+1}^N \mathcal{P}_l$ , respectively.  $N$  is the total number of packets in the image, assumed to be even. Two bytes of cyclic redundancy check (CRC) is appended to the  $b_s^{(l)}$  bits of information for  $\mathcal{P}_l$ , where  $l = 1, 2, \dots, N$ , along with  $m$  additional bits to flush the memory and terminate the decoding trellis in the all-zero state. A total of  $b_s^{(l)} + 16 + m$  bits are then encoded using RCPC code rate  $\omega_l$  for packet  $l$ . Packets are ordered and modulated using one of the packetization and hierarchical modulation techniques described in Section III. Finally, the output symbol stream is sent through the wireless channel. Perfect channel state information (CSI) is assumed at the receiver. It is used to determine the optimal parameters of the system. Finally, the hierarchical demodulator receives the optimized parameter information, demodulates the incoming symbols, and decodes the codewords using a Viterbi decoder. In the proposed setting, the receiver is assumed to feed the channel parameters back to the transmitter over a reliable channel. In practice, the channel parameters are encoded with heavy protection and placed in packet header sections. We assume that there is no significant loss in throughput due to the transmission of the CSI.

We define the vectors  $\mathbf{d} := [d_0, d_1, \dots, d_l, \dots, d_N]$  and  $\mathbf{r} := [R_1, R_2]$ , where  $R_1$  and  $R_2$  are the code rates of the first and second halves of the packets. In other words, we use  $R_1$  for the

bits in  $\mathcal{P}'_{\cup}$  ( $\omega_l = R_1$  for  $l = 1, \dots, N/2$ ) and  $R_2$  to protect the bits in  $\mathcal{P}''_{\cup}$  ( $\omega_l = R_2$  for  $l = N/2 + 1, \dots, N$ ). As will be clear in Section III, the packetization and combining strategy using only hierarchical modulation puts a natural constraint on the bit error rate (BER) performance of the bits in  $\mathcal{P}''_{\cup}$  and  $\mathcal{P}'_{\cup}$ . That is, once a hierarchical parameter is selected to achieve the target HP BER, it will also determine the LP BER. The idea of using two different channel code rates is to alleviate this constraint and make the system more flexible in terms of assigning target BERs.

We use a finite discrete set of RCPC codes  $C_r = \{c_1, c_2, \dots, c_n\}$  [20]. Our system uses packets of  $\nu$  bits with code rates  $R_1 = a_1/b_1$  and  $R_2 = a_2/b_2$ , with  $\text{g.c.d}\{a_1, b_1\} = \text{g.c.d}\{a_2, b_2\} = 1$ . The following procedure is used to determine the packet size, given  $R_1$  and  $R_2$ . We begin with a nominal value  $\nu_m$ . If  $\nu_m$  is divisible by  $\text{l.c.m}\{b_1, b_2\}$ , then the packet size  $\nu = \nu_m$  is used. Otherwise, we use  $\nu = \lfloor \nu_m / \text{l.c.m}\{b_1, b_2\} \rfloor \cdot \text{l.c.m}\{b_1, b_2\}$ , where  $\lfloor \cdot \rfloor$  is the floor function. For a given transmission rate  $r_{\text{tr}}$  in bits per pixel (bpp), the number of packets is  $N = \lfloor (r_{\text{tr}} \times L_x \times L_y) / \nu \rfloor_{\text{even}}$ , where  $\lfloor \cdot \rfloor_{\text{even}}$  rounds down to the nearest even integer. The source rate  $r_s$  in bpp is given by  $r_s = \sum_l b_s^{(l)} / L_x \times L_y$ , where  $b_s^{(l)} = \nu r_l - 16 - m$ .

For a given  $\mathbf{r}$ , first,  $\mathbf{d}$  is determined and used in our optimization algorithm to construct the optimal hierarchical parameters ( $\alpha^* := [\alpha_1^*, \alpha_2^*, \dots, \alpha_{N/2}^*]$ ). Then, we optimize over all possible  $(R_1, R_2)$  to find  $\mathbf{r}^* = [R_1^*, R_2^*]$ . The optimal parameters  $\{\alpha^*, \mathbf{r}^*\}$  are chosen to minimize the reconstructed source distortion at the receiver, as will be discussed later.

### III. BIT-TO-SYMBOL ASSIGNMENT METHODOLOGIES

Different bit-to-symbol assignment strategies will be called packetization [21]. We consider two combining strategies: 1) folded packetization *FP* and 2) sequential packetization *SP*. As shown in Fig. 3(a), for *FP*,  $\alpha_i$  with  $i = 1, 2, \dots, N/2$  is used to combine bits in  $\mathcal{P}_i$  and  $\mathcal{P}_{N-i+1}$ . This means that for  $z = 1, \dots, \nu$ , the  $z$ th bit of  $\mathcal{P}_i$  and the  $z$ th bit of  $\mathcal{P}_{N-i+1}$  are encoded together using, say, the H-4PAM ( $\alpha_i$ ) constellation to produce the modulated symbols. We use hierarchical parameters  $\{\alpha_i \in \mathbb{R} : \alpha_i \in [t_i, u_i]\}$ , where  $t_i$  and  $u_i$  are lower and upper bounds, respectively, for  $\alpha_i$ . For *SP*, as shown in Fig. 3(b),  $\alpha_{(k+1)/2}$  is used to combine bits in  $\mathcal{P}_k$  and  $\mathcal{P}_{k+1}$ ,

where  $k = 1, 3, 5, \dots, N - 1$ . The assignment strategy for  $FP$  is originally used in [22] and is called packet reversed packet combining in [23], where the bits are encoded using XOR operation (bit combining). The idea was to correct bit errors in automatic repeat request (ARQ) through multiple transmissions of the same message. The same assignment strategy is utilized in conjunction with hierarchical modulation in [24]. It is used with channel coding and hierarchical modulation in [25] for AWGN and flat Rayleigh fading channels.

An error in a progressive coded bit stream leaves the remaining part of the stream undecodable [2], [3], [7]. Therefore, in case of an error, the encoded stream is truncated, and the decoded packets are used to reconstruct the source. If we consider fixed length packets, then the number of information bits ( $b_s^{(l)}$ ) within each packet varies based on the channel code rate used. The optimized system assigns the set of hierarchical parameters  $\alpha^*$  to determine the relative reliability among the packets. Previous UEP JSCC techniques protect the progressive stream using a discrete set of channel code rates. If the optimal protection can be provided with a code that falls in between two available code rates in the set, then the closest one is chosen to protect the packet [2]. In our system, UEP is flexibly provided using both a discrete code set and continuous-valued hierarchical parameters throughout the progressive bit stream.

#### IV. PERFORMANCE ANALYSIS

In this section, we describe the distortion minimization framework for our system and give packet error rate (PER) expressions for RCPC codes. A lower bound for the system performance improvement over equal error protection (EEP) is analytically derived, and numerical results are given to support the argument. We assume ideal coherent detection and perfect CRC error detection.

Let  $\rho_l(\gamma)$  be the average bit error probability for the  $l$ th packet as a function of  $\gamma = E_b/N_0$ , where  $E_b$  is the average bit energy, and  $N_0$  is the power spectral density of the noise, and assume the all-zero codeword is transmitted. For a given code rate  $\beta \in C_r$ , let  $\delta^{(\beta)}$  represent the distance to the all-zero codeword of the path being compared with the all-zero path at some node in the trellis. For a BSC with crossover probability  $\rho_l(\gamma)$ , the probability of selecting the incorrect path is given by [28]

$$P_{\delta^{(\beta)}}^l = \begin{cases} \sum_{j=\frac{\delta^{(\beta)}}{2}+1}^{\delta^{(\beta)}} \binom{\delta^{(\beta)}}{j} (1-\rho_l(\gamma))^{\delta^{(\beta)}-j} \rho_l^j(\gamma), & \text{if } \delta^{(\beta)} \text{ odd} \\ \sum_{j=\frac{\delta^{(\beta)}}{2}+1}^{\delta^{(\beta)}} \binom{\delta^{(\beta)}}{j} (1-\rho_l(\gamma))^{\delta^{(\beta)}-j} \rho_l^j(\gamma) \\ + \binom{1}{2} \frac{\delta^{(\beta)}}{\delta^{(\beta)}/2} (1-\rho_l(\gamma))^{\delta^{(\beta)}/2} \rho_l^{\delta^{(\beta)}/2}(\gamma), & \text{if } \delta^{(\beta)} \text{ even.} \end{cases} \quad (2)$$

The number of distinct values of  $P_{\delta^{(\beta)}}^l$  is equal to the number of different BERs that can be provided by the hierarchical  $M$ -ary constellation. For example, in 4-PAM, we need to compute (2) for two BERs, which are given for AWGN ( $\rho^{HP}(\alpha, \gamma)$ ,  $\rho^{LP}(\alpha, \gamma)$ ) in (3) and (4), shown below, and for

flat Rayleigh fading channels ( $\rho_{Ray}^{HP}(\alpha, \gamma)$ ,  $\rho_{Ray}^{LP}(\alpha, \gamma)$ ) in (5) and (6) [26], shown below, i.e.,

$$\rho^{HP}(\alpha, \gamma) = \frac{1}{2} \left[ Q \left( \sqrt{\frac{8\gamma}{1+\alpha^2}} \right) + Q \left( \sqrt{\frac{8\gamma\alpha^2}{1+\alpha^2}} \right) \right] \quad (3)$$

$$\rho^{LP}(\alpha, \gamma) = \frac{1}{2} + \frac{1}{2} \sum_{s=0}^1 \sum_{m=0}^1 (-1)^{s+m} \times Q \left( \left[ \frac{(-1)^s(1+\alpha)}{2} + \alpha^m \right] \sqrt{\frac{8\gamma}{1+\alpha^2}} \right) \quad (4)$$

where  $Q(x) = \frac{1}{\sqrt{2\pi}} \int_x^{\infty} e^{-\frac{z^2}{2}} dz$

$$\rho_{Ray}^{HP}(\alpha, \gamma, \sigma) = \frac{1}{2} - \frac{1}{4} \sqrt{\frac{\lambda}{1+\lambda}} - \frac{1}{4} \sqrt{\frac{\alpha^2\lambda}{1+\alpha^2\lambda}} \quad (5)$$

where  $\lambda = \frac{8\sigma^2\gamma}{(1+\alpha^2)}$

$$\rho_{Ray}^{LP}(\alpha, \gamma, \sigma) = \frac{1}{2} + \frac{1}{2} \sum_{s=0}^1 \sum_{m=0}^1 (-1)^{s+m} \left( \frac{1}{2} - \frac{\text{sgn}(\tilde{\Omega})}{2\sqrt{1+\frac{1}{\lambda}}} \right) \quad (6)$$

where  $\tilde{\Omega} = \frac{(-1)^s(1+\alpha)}{2} + \alpha^m$ ,  $\tilde{\gamma} = \tilde{\Omega}^2\lambda$

Depending on the symbol sent, the BERs for a particular bit location can be quite different. For example, using H-4PAM, we can have different BERs for HP bits, depending on the values of  $\alpha$  and the LP bits. We use  $\epsilon_1$  to denote the BER for the HP bit if the LP bit is 0, and  $\epsilon_2$  denotes the BER for the HP bit if the LP bit is 1, where  $(\epsilon_1, \epsilon_2)$  can be given for AWGN and flat independent Rayleigh channels as [26]

$$(\epsilon_1, \epsilon_2) = \begin{cases} \text{AWGN} : & \left( Q \left( \sqrt{\frac{8\gamma}{1+\alpha^2}} \right), Q \left( \sqrt{\frac{8\gamma\alpha^2}{1+\alpha^2}} \right) \right) \\ \text{Rayleigh} : & \left( \frac{1}{2} - \frac{1}{2} \sqrt{\frac{\lambda}{1+\lambda}}, \frac{1}{2} - \frac{1}{2} \sqrt{\frac{\alpha^2\lambda}{1+\alpha^2\lambda}} \right) \end{cases}$$

where  $\lambda = 8\sigma^2\gamma/(1+\alpha^2)$ ,  $\gamma (= E_b/N_0)$  is the average signal-to-noise ratio (SNR) per bit,  $\alpha$  is the hierarchical parameter,  $Q(z) = (1/\sqrt{2\pi}) \int_z^{\infty} e^{-(x^2/2)} dx$ , and  $\sigma$  is the parameter of the Rayleigh probability density function, which is given by  $f(x; \sigma) = (x/\sigma^2) e^{-x^2/2\sigma^2}$ .

Note that since the LP bits are equally likely to be 0 or 1, the average BERs of the HP bits given in (3) and (5) for the AWGN and flat Rayleigh are simply given by  $(1/2)(\epsilon_1 + \epsilon_2)$ . Thus, the channel to which the bits of the H-4PAM symbol are exposed can be modeled as a two-state channel with transition probabilities 0.5, 0.5, where the channel in one state is a BSC with crossover probability  $\epsilon_1$ , and the channel in the other state is a BSC with crossover probability  $\epsilon_2$ . We can also generate a similar set of error probabilities for LP bits. It can be shown that (2) is applicable for  $M$ -ary hierarchical modulation, if the channel for each bit location can be modeled as a two-state channel [27].

### A. PER Approximation

Let us define  $(\overline{Q}_b^l)$  to be the union bound for the average bit error probability for the bits in packet  $l$  [28]. Using the formulation in [29], the PER for packet  $l$  ( $\text{PER}_l$ ) can be upper bounded by

$$\text{PER}_l \leq 1 - \left( 1 - \frac{1}{p} \sum_{\delta^{(\beta)} = \delta_{\text{free}}}^{\infty} c_{\delta^{(\beta)}} P_{\delta^{(\beta)}}^l \right)^{b_s^l} \quad (7)$$

where  $p$  is the puncturing period,  $\delta_{\text{free}}$  is the free distance of the code, and  $c_{\delta^{(\beta)}}$  is the coefficient of the bit input weight enumeration function of a given code  $\beta \in C_r$  [20].

In this formulation, the bounds derived can be very loose, especially at low SNR values. Therefore, we use a nonlinear least square regression (NLSR) technique to approximate  $\text{PER}_l$  in (7). For packet  $l$ , the approximation is  $\widehat{\text{PER}}_l = 1 - A^* e^{B^* \times \overline{Q}_b^l}$ , where  $A^*$  and  $B^*$  are parameters chosen according to the following criterion:

$$(A^*, B^*) = \arg \min_{A, B \in \mathbb{R}} \left\{ \sum_{j=1}^s \left| \overline{\text{PER}}_l^{(\gamma_j)} - \left( 1 - A \times e^{B \times \overline{Q}_b^l(\gamma_j)} \right) \right|^2 \right\} \quad (8)$$

where  $s$  is the number of SNR values used in the approximation, and  $\overline{\text{PER}}_l^{(\gamma_j)}$  is the average PER for packet  $l$ , meaning the expected value of the random variable that is the outcome of a Monte Carlo simulation at each average SNR  $\gamma_j$ . Note that the actual PER is a random variable since, averaged over all the channel and noise realizations, the  $\overline{\text{PER}}_l^{(\gamma_j)}$  is defined to be the number of packets in error divided by the total number of packets received at an SNR  $\gamma_j$ . In addition,  $\overline{Q}_b^l(\gamma_j)$  is the hard decision upper bound for the bit error probability evaluated at each  $\gamma_j$ . Finally,  $\{\gamma_j\}_{j=1}^s$  is the set of average SNR values we use to apply NLSR to have a good functional approximation to the simulated average PER values ( $\{\overline{\text{PER}}_l^{(\gamma_j)}\}_{j=1}^s$ ) over the range  $[\min\{\gamma_j\}, \max\{\gamma_j\}]$ . Based on our experimental observation,  $s = 10$  for the SNRs of interest yields an accurate estimate [i.e.,  $A^*$  and  $B^*$  of the functional approximation in (8)].

For example, we simulated coded conventional 4PAM and 16QAM (i.e.,  $\alpha = 3$ ) using  $FP$  and a packet size of 450 bits with the code rate  $\beta = 1/2$  and plot PER versus SNR per bit (see Figs. 4 and 5) for both HP and LP packets, assuming the same average power per constellation. The NLSR better matches the simulation results for the range of SNRs of interest. This functional approximation will be helpful later in formulating the cost function, which needs to be minimized.

### B. Construction of the Optimization Problem

For a given  $\gamma$  and  $\mathbf{r}$ , we want to select vector  $\alpha^*$  so as to minimize the expected distortion  $\overline{D}_\alpha$ . Assuming independent

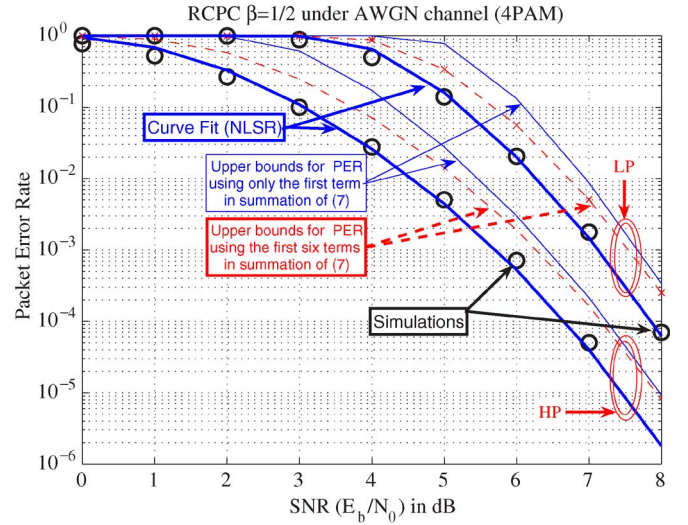


Fig. 4. Proposed NLSR versus simulation results and upper bounds derived in this paper for both HP and LP priority classes using 4PAM and an RCPC code rate  $\beta = 1/2$ .

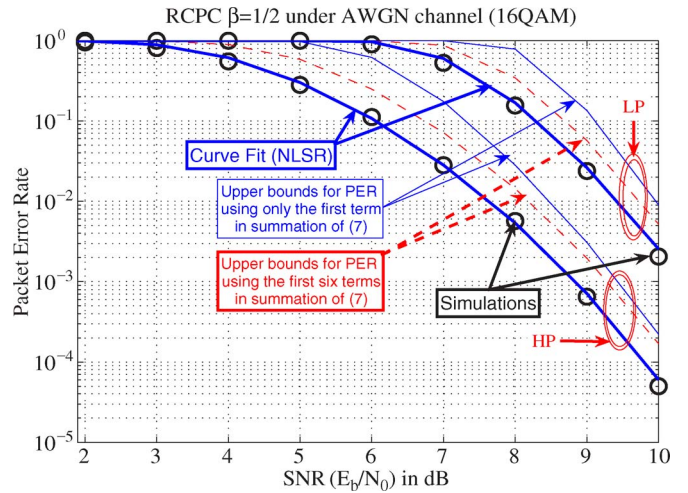


Fig. 5. Proposed NLSR versus simulation results and upper bounds derived in this paper for both HP and LP priority classes using 16QAM and an RCPC code rate  $\beta = 1/2$ .

packet losses, it can be shown that  $\overline{D}_\alpha$  can be expressed (for both  $FP$  and  $SP$ ) as [30]

$$\begin{aligned} \overline{D}_\alpha &= \sum_{l=0}^N \widehat{\text{PER}}_{l+1} \prod_{i=0}^l (1 - \widehat{\text{PER}}_i) d_l \\ &= d_0 - \sum_{l=1}^N \prod_{i=1}^l (1 - \widehat{\text{PER}}_i) \Delta_l \end{aligned} \quad (9)$$

where  $\widehat{\text{PER}}_{l+1} \prod_{i=0}^l (1 - \widehat{\text{PER}}_i)$  is the probability of having the first  $l$  packets correct, and we have an error in the  $(l+1)$ th packet, and  $\Delta_l = d_{l-1} - d_l \geq 0$  is the amount that the distortion is reduced by having the  $l$ th packet received error free, given that all the previous  $l-1$  packets were reliably received. We define  $\widehat{\text{PER}}_0 = 0$  and  $\widehat{\text{PER}}_{N+1} = 1$ . Note that  $\widehat{\text{PER}}_l$  depends on the average BER bound  $(\overline{Q}_b^l)$ , which is a

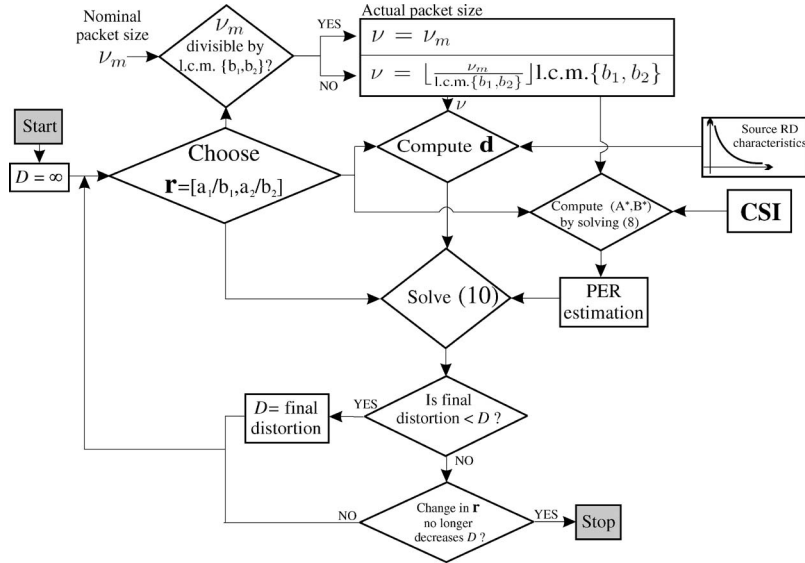


Fig. 6. Functional flow diagram of the proposed optimization scheme.

function of the channel code rate and the hierarchical modulation parameters. Our optimization problem is given by

$$\min_{\substack{\mathbf{r} \\ \omega_l \in C_r \\ l=1, \dots, N}} \left\{ \min_{\alpha_i} \bar{D}_\alpha \right\} \quad \text{subject to } t_i \leq \alpha_i \leq u_i \quad (10)$$

where  $t_i \in \mathbb{R}$  and  $u_i \in \mathbb{R}$  are lower and upper bounds for the hierarchical parameter  $\alpha_i$ , respectively. Since we have  $d_0 \geq 0$ , we can rewrite the previous expression using (9) as

$$\min_{\substack{\mathbf{r} \\ \omega_l \in C_r \\ l=1, \dots, N}} \left\{ \min_{\alpha_i} \left\{ \sum_{l=1}^N \xi_{\omega_l, l} \Delta_l \right\} \right\} \quad \text{s.t. } t_i \leq \alpha_i \leq u_i \quad (11)$$

where  $\xi_{\omega_l, l} = -\prod_{i=1}^l (1 - \widehat{\text{PER}}_i)$ .

### C. Optimization of Hierarchical Parameter Set $\alpha$

Starting with the discrete code set, for each choice of  $\mathbf{r}$ , we optimize the hierarchical parameters for that value of  $\mathbf{r}$ . After exhausting all the values of  $\mathbf{r}$  in the set, we obtain the optimal code rate vector  $\mathbf{r}^*$  with the corresponding optimal hierarchical parameters that give the minimum distortion. More specifically, for each  $\mathbf{r}$ , we determine  $\alpha^*$  by solving (10). Note that it would be possible to approach this iteratively: for a given  $\mathbf{r}$ , find the corresponding optimal  $\alpha^*$ , and then given  $\alpha^*$ , determine  $\mathbf{r}^*$  by solving (10) for  $\mathbf{r}$ , etc. However, we avoided this iterative approach because it can result in a local minimum and be complex.<sup>1</sup> Instead, for each element of a constrained set of code rates, we solve for  $\alpha^*$  and in the end obtain the global optimum.

Using (11), our optimization problem is given by

$$\min_{\substack{\mathbf{r} \\ \omega_l \in C_r \\ l=1, \dots, N}} \left\{ \min_{\alpha_i} \left\{ \sum_{l=1}^N \xi_{\omega_l, l} \Delta_l \right\} \right\} \quad \text{s.t. } g_l \leq x_l \quad (12)$$

<sup>1</sup>Since the number of code rates in  $C_r$  is discrete, the latter optimization procedure is an integer programming which is computationally complex (NP-hard).

where

$$g_l = \begin{cases} \alpha_l & 1 \leq l \leq N/2 \\ -\alpha_{l-N/2} & \frac{N}{2} + 1 \leq l \leq N \end{cases}$$

$$x_l = \begin{cases} u_l & 1 \leq l \leq N/2 \\ -t_{l-N/2} & \frac{N}{2} + 1 \leq l \leq N. \end{cases}$$

The Lagrangian function of (12) can be written as [31]

$$\Lambda_D(\alpha) = \Lambda(\alpha_1, \alpha_2, \dots, \alpha_{N/2}, \lambda_1, \dots, \lambda_N)$$

$$= \sum_{l=1}^N \xi_{\omega_l, l} \Delta_l - \lambda_l (g_l - x_l) \quad (13)$$

where the parameters  $\lambda_1, \lambda_2, \dots, \lambda_N$  are the Lagrange multipliers. The unconstrained minimization problem is  $\min_{\mathbf{r}} \min_{\alpha} \{\Lambda_D(\alpha)\}$ . The necessary conditions for our optimization problem are given by the Karush–Kuhn–Tucker (KKT) conditions

$$\nabla \Lambda_D(\alpha^*) = \left[ \frac{\partial \Lambda_D}{\partial \alpha_1^*}, \dots, \frac{\partial \Lambda_D}{\partial \alpha_{N/2}^*}, \frac{\partial \Lambda_D}{\partial \lambda_1^*}, \dots, \frac{\partial \Lambda_D}{\partial \lambda_N^*} \right] = 0 \quad (14)$$

with  $\lambda_l^* (g_l^* - x_l) = 0$ ,  $\lambda_l^* \geq 0$ , and  $t_i \leq \alpha_i^* \leq u_i$ . We use numerical approaches to solve the set of nonlinear equations in (14) for the  $\alpha^*$  that minimizes  $\bar{D}_\alpha$  [32]. In addition, in [33], the KKT conditions are derived in a similar to the way we derive our KKT conditions for a convex cost function and convex constraints. Descriptions of the system components as well as the optimization procedure given in Sections II–IV are summarized in a diagram in Fig. 6.

### D. Lower Bound on the Performance Improvement of the Proposed System

We denote the general hierarchical parameter set  $\alpha := \{\alpha_i \in \mathbb{R}\}_{i=1}^{N/2}$  and use  $\alpha_a := \{\alpha_i = a\}_{i=1}^{N/2}$  when all the hierarchical

parameters have the same real value  $a \in \mathbb{R}$ . For example,  $\alpha_3$  means that all the hierarchical parameters have the value 3; this corresponds to conventional modulation. As a baseline for comparison, we consider an EEP scheme that uses *SP* and conventional modulation, i.e.,  $\alpha_3$ .

*Proposition 1:* We can order the expected distortions of the systems as follows:

$$\begin{aligned} \mathbb{E}[\mathcal{D}^{SP}(R^*, R^*, \alpha_3)] &\geq \mathbb{E}[\mathcal{D}^{FP}(R^*, R^*, \alpha_3)] \\ &\geq \mathbb{E}[\mathcal{D}^{FP}(R_1^*, R_2^*, \alpha_{\alpha^*})] \\ &\geq \mathbb{E}[\mathcal{D}^{FP}(R_1^*, R_2^*, \alpha^*)] \end{aligned} \quad (15)$$

where  $\mathcal{D}^j(R_1, R_2, \alpha)$  is the distortion using packetization  $j \in \{SP, FP\}$ , channel code rates  $R_1$  and  $R_2$  for the first and second halves of the packet stream, respectively, and hierarchical parameter set  $\alpha$ . The EEP system uses  $R^*$  as the single optimal code rate. For the system that uses *FP* and a single optimal hierarchical parameter  $\alpha^*$ ,  $(R_1^*, R_2^*)$  is the optimal rate pair, and  $\alpha_{\alpha^*}$  is the vector of identical hierarchical parameters  $\alpha^*$ .

*Proof:* The second inequality in (15) follows because optimal parameters  $(R_1^*, R_2^*, \alpha_{\alpha^*})$  minimize the expected distortion. The third inequality arises because we increase the parameter space from 3 to  $(N/2) + 2$  and optimize each parameter value. Therefore, we need to show only the first inequality in (15).

We show in the Appendix that

$$\begin{aligned} \Delta\mathcal{D}_N(\alpha_3; \Omega) &\triangleq \mathbb{E}[\mathcal{D}^{SP}(R^*, R^*, \alpha_3)] \\ &\quad - \mathbb{E}[\mathcal{D}^{FP}(R^*, R^*, \alpha_3)] \geq 0. \end{aligned} \quad (16)$$

We define the total distortion measure  $\mathcal{D}_N^j(\alpha; \mathcal{A}) := -\sum_{l \in \mathcal{A}} \prod_{i=1}^l P_i \Delta_l$  using only the bits in a given set  $\mathcal{A}$  and using packetization  $j \in \{SP, FP\}$  in an  $N$ -packet error protection scheme, where  $\alpha = [\alpha_1 \ \alpha_2, \dots, \alpha_{N/2}]$ . In addition,  $P_i = 1 - \overline{\text{PER}}_i$  is the probability of receiving packet  $i$  reliably. From (9), for packetization  $j$ , we have  $\overline{D}_\alpha = d_0 + \mathcal{D}_N^j(\alpha; \Omega)$ , where  $\Omega = \mathcal{P}'_U \cup \mathcal{P}''_U$ . Finally, the peak SNR (PSNR) gap ( $\Delta\text{PSNR}$ ) between systems using *FP* and *SP* is given by

$$\begin{aligned} \Delta\text{PSNR} &\triangleq 10 \log \frac{255^2}{\mathbb{E}[\mathcal{D}^{FP}(R^*, R^*, \alpha_3)]} \\ &\quad - 10 \log \frac{255^2}{\mathbb{E}[\mathcal{D}^{SP}(R^*, R^*, \alpha_3)]} \\ &= 10 \log \frac{255^2}{d_0 + \mathcal{D}_N^{FP}(\alpha_3; \Omega)} \\ &\quad - 10 \log \frac{255^2}{d_0 + \mathcal{D}_N^{SP}(\alpha_3; \Omega)} \\ &= 10 \log \frac{d_0 + \mathcal{D}_N^{SP}(\alpha_3; \Omega)}{d_0 + \mathcal{D}_N^{FP}(\alpha_3; \Omega)} \\ &= 10 \log \frac{d_0 + \mathcal{D}_N^{SP}(\alpha_3; \Omega)}{d_0 + \mathcal{D}_N^{SP}(\alpha_3; \Omega) - \Delta\mathcal{D}_N(\alpha_3; \Omega)} \geq 0 \end{aligned} \quad (17)$$

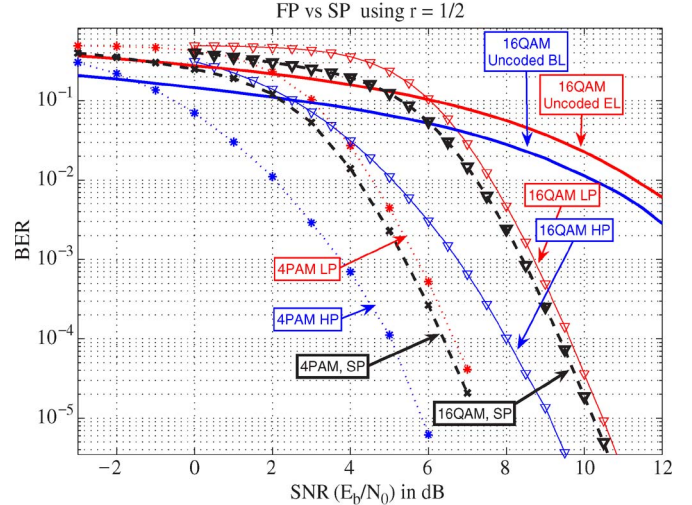


Fig. 7. HP and LP BER performances using uncoded and coded ( $r = 1/2$ ) conventional 4PAM/16QAM for AWGN channel.

where  $\Delta\mathcal{D}_N(\alpha_3; \Omega) = \mathcal{D}_N^{SP}(\alpha_3; \Omega) - \mathcal{D}_N^{FP}(\alpha_3; \Omega) = \mathbb{E}[\mathcal{D}^{SP}(R^*, R^*, \alpha_3)] - \mathbb{E}[\mathcal{D}^{FP}(R^*, R^*, \alpha_3)] \geq 0$  by Proposition 1. From (15), we have

$$\begin{aligned} \mathbb{E}[\mathcal{D}^{SP}(R^*, R^*, \alpha_3)] - \mathbb{E}[\mathcal{D}^{FP}(R_1^*, R_2^*, \alpha_{\alpha^*})] \\ \geq \mathbb{E}[\mathcal{D}^{SP}(R^*, R^*, \alpha_3)] - \mathbb{E}[\mathcal{D}^{FP}(R^*, R^*, \alpha_3)] \\ = \Delta\mathcal{D}_N(\alpha_3; \Omega) \geq 0. \end{aligned} \quad (18)$$

Thus,  $\Delta\text{PSNR}$  is a lower bound for the performance improvement of the proposed system over the EEP scheme.

### E. Numerical Results for Memoryless Channels

Our first simulation demonstrates the average BER performances of different packetized bit-to-symbol assignments. We present simulation results for the coded cases and numerical computation of BER expressions for the uncoded case. We consider both H-4PAM and H-16QAM, and assume the same average power per constellation. Figs. 7 and 8 show the performance of different packetization schemes using conventional modulation. There is a BER gap between uncoded HP bits and LP bits, which is inherent to PAM signaling and, therefore, to higher QAM constellations. This gap widens when we use lower channel code rates, because parity bits are also protected unequally. There is no gap in SP because the average HP BER is equal to the average LP BER.

Next, we apply code rates  $R_1$  and  $R_2$  for the first and second halves of the total packet stream i.e.,  $\mathbf{r} = [R_1 \ R_2]$ . We initially use  $\nu_m = 450$  bits (we will later look at different values of  $\nu_m$ ) and the RCPC code set with constraint length  $K = 7$  from [20]: The code rate set is  $C_r = \{8/9, 4/5, 2/3, 4/7, 1/2, 4/9, 2/5, 4/11, 1/3, 4/13, 2/7, 4/15, 1/4\}$ . A CRC code from [3] is used for error detection. Standard grayscale (8 bpp) images *Lena* ( $512 \times 512$ ), *Barbara* ( $512 \times 512$ ), *Goldhill* ( $512 \times 512$ ), *Peppers* ( $512 \times 512$ ), and *Baboon* ( $512 \times 512$ ) are encoded using the SPIHT and JPEG2000 [34] algorithms. For space limitations, we only show the results for *Lena* and *Barbara* using SPIHT. For the other images, the proposed scheme shows similar performance gains. The transmission rate

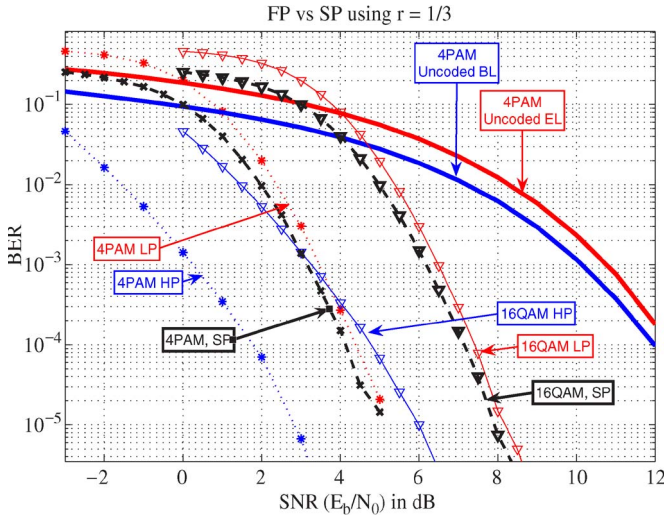


Fig. 8. HP and LP BER performances using uncoded and coded ( $r = 1/3$ ) conventional 4PAM/16QAM for AWGN channel.

$r_{tr}$  is 0.25 bpp. For roughly  $10^4$  different channel realizations, we simulate the system/s to obtain MSE values. We then average the MSE values before converting to average PSNR. In the proposed system, hierarchical parameters and channel code rates are found by solving the optimization problem. We introduce the following systems:

- 1) seqConv1: *SP*, conventional modulation. One optimal code rate chosen from  $C_r$ ;
- 2) foldConv1: *FP*, conventional modulation. One optimal code rate chosen from  $C_r$ ;
- 3) foldHier1: *FP*, hierarchical modulation ( $\alpha^*$ ). One optimal code rate chosen from  $C_r$ ;
- 4) foldHier2: *FP*, hierarchical modulation ( $\alpha^*$ ). Two optimal code rates chosen from  $C_r$ .

We ignore the other four combinations: 1) seqConv2; 2) seqHier1; 3) seqHier2; and 4) foldConv2. First of all, combining *SP* and hierarchical modulation is not useful because consecutive packets bear almost the same significance in terms of end-to-end distortion. In addition, by switching from *SP* to *FP*, foldConv2 gives a lower distortion than seqConv2. Finally, note that foldConv2 is a special case of foldHier2 when  $\alpha = \alpha_3$ . Thus, the performance of those systems is not shown.

Note that seqConv1 is an EEP scheme because it assigns a fixed average BER (which corresponds to  $\alpha_3$ ) for every pair of packets. Fig. 9 shows the performance of various systems. The UEP schemes always perform better than the EEP scheme. The nonconcave behavior of these curves is a consequence, at least in part, of  $C_r$  being discrete. In addition to this constraint, our design constraint is that the  $\alpha$  values determine the BER for each packet in the first and second halves of the packet stream simultaneously. However, the foldHier2 system somewhat alleviates both constraints by employing two different code rates for the two halves of the stream. We also observe a slight performance improvement when we use more than two channel code rates at the expense of greater complexity.

The optimal hierarchical values  $\alpha^*$  as a function of packet index (PI) are plotted in Fig. 10 for the first half of the stream. The figure shows that  $\alpha_1 \leq \alpha_2 \leq \dots \leq \alpha_{N/2}$ , meaning that

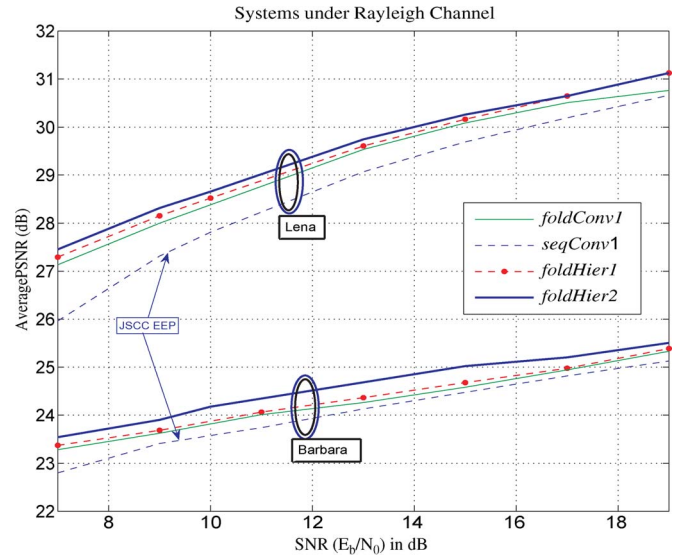


Fig. 9. Performance of different systems for an independent flat Rayleigh fading channel. JSCC EEP is also drawn for comparison. This figure uses the approximate PER expressions obtained by nonlinear regression for both *Lena* and *Barbara* images.

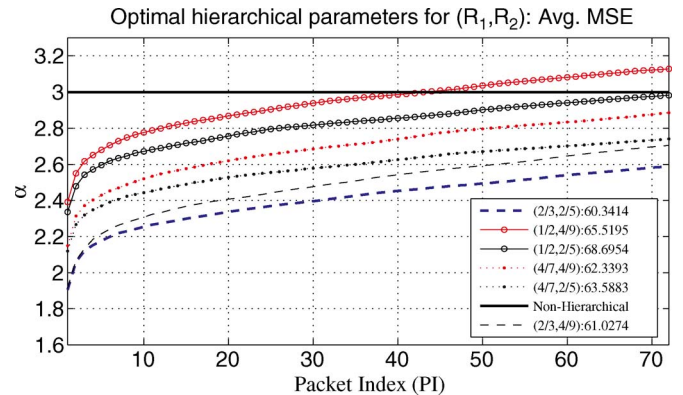


Fig. 10. Optimal hierarchical parameters ( $\alpha^*$ ) for different channel code rate pairs at SNR = 7 dB for an AWGN channel. It also shows the corresponding calculated values of MSE. (2/3, 2/5) is the optimal code rate pair.

earlier packets in the stream are more heavily protected by the hierarchical modulation. The discrete nature of the code set is the cause of nonuniform gains going from one UEP scheme to another, and the cause of different gains at different SNRs. At low SNRs, the gap between the curves becomes more pronounced as UEP is more effective when the channel degrades.

Another interesting observation is that  $R_1 \geq R_2$  for foldHier2. However, in a JSCC-only UEP scheme [2], we would expect  $R_1 \leq R_2$  [30], i.e., we would expect to protect the first part more heavily than the second part. This is not the case when JSCC is used with hierarchical modulation simply because the hierarchical parameters adjust themselves to protect the bits of the first half more than the bits of the remaining half. As long as these parameters are able to compensate for the decreased protection due to the FEC,  $R_1 \geq R_2$  can improve the system performance by allocating more information bits in the first half of the packets, where the favorable hierarchical modulation parameters ensure their reliable transfer. This leads to better reconstruction quality.

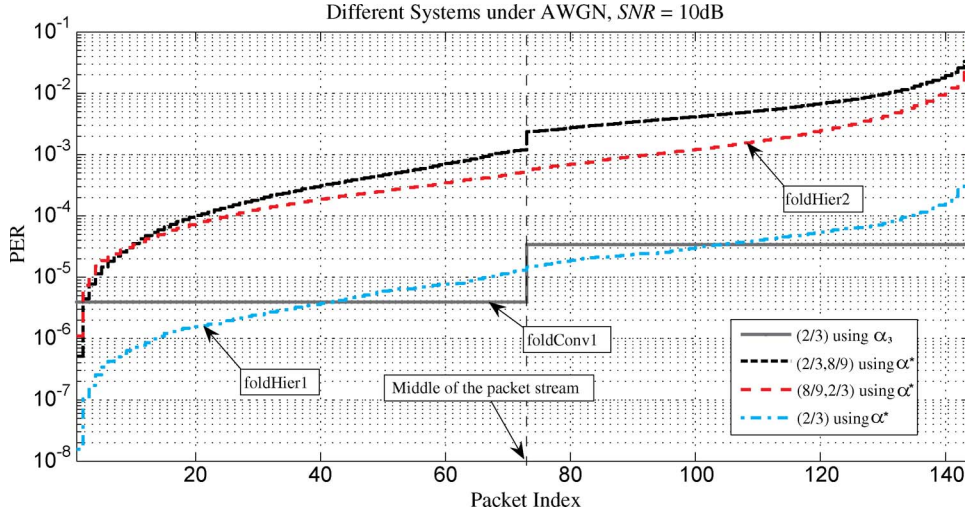


Fig. 11. PER assignment among the packets of  $\alpha$ -adaptive system can provide hundreds of different UEP levels, whereas UEP achieved by packetization provides only two layers of unequal PERs.

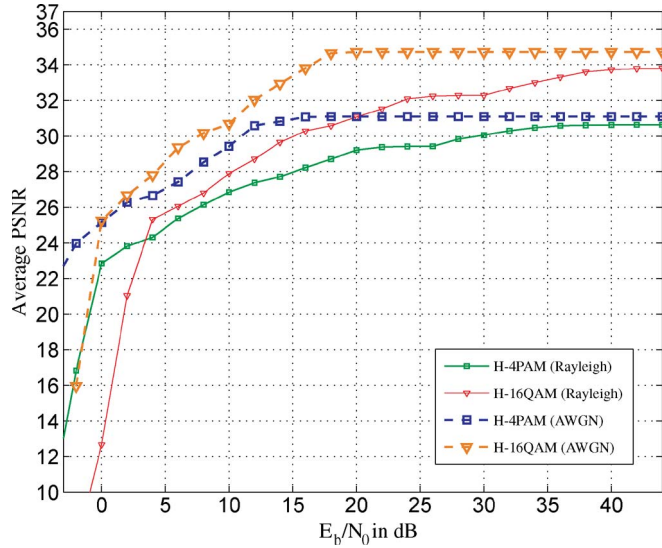


Fig. 12. Proposed system using H-4PAM, H-16QAM constellations, and the corresponding upper bounds for  $PER_l$  given in (7) in the formulation of the cost function instead of using the approximation  $\widehat{PER}_l, l = 1, 2, \dots, N$  and the optimal values in (8). Since upper bounds give higher PERs compared with the approximation we use, those PSNR performance curves can be thought of as lower bounds for the actual performance of the proposed system.

In Fig. 11, PER as a function of PI number is shown at  $SNR = 10$  dB with both the optimal pair of codes and one with reverse order. The case where  $R_1 \geq R_2$  is seen to protect almost all the packets better than the  $R_2 \geq R_1$  case. Finally, the system can provide as many UEP levels as the number of packets, although the system uses only two code rates. The step jump for foldConv1 is due to the natural BER gap between HP and LP bits when we use  $\alpha_3$  and the channel coding (since the channel coding increases this gap). On the other hand, the step jump in the system using code rate pair (2/3, 8/9) is due to the different channel code rates with different protection capabilities. In addition, for this system, adaptive hierarchical parameters cannot compensate for the performance gap due solely to channel coding. In foldHier2, however, this gap due to different channel code rates is compensated with adaptive

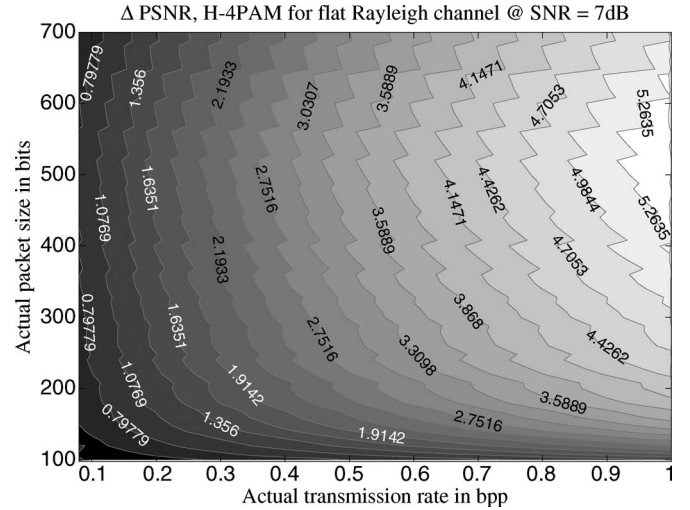


Fig. 13. Performance upper bound is calculated for different transmission rates (in bpp) and packet sizes, illustrating the effect of transmission rate and packet size on the proposed system.

hierarchical parameters, and we observe no step jump in the PER performance.

We have also considered the H-16QAM constellation. To begin, we choose  $r_{tr} = 0.15$  bpp for H-4PAM and let the two constellations have the same average power. Since H-16QAM transmits twice the number of bits of H-4PAM in a given unit time, the effective transmission rate is doubled, i.e.,  $r_{tr} = 0.3$  bpp for the H-16QAM system. Fig. 12 shows the foldHier1 system using different hierarchical modulations for an independent flat Rayleigh fading channel.

Finally, we present the numerical calculation results of the performance improvement lower bound ( $\Delta PSNR$ ) given in (16) to find the effect of transmission rate ( $r_{tr}$ ) in bpp and the packet size in bits (which previously in this paper were taken to be 0.25 bpp and  $\sim 450$  bits, respectively) of the proposed system. For a flat Rayleigh fading channel using H-4PAM at  $SNR = 7$  dB,  $\Delta PSNR$  is calculated and plotted in Fig. 13 as a function of packet size and  $r_{tr}$ . The jagged curves are contours along which  $\Delta PSNR$  is the same up to four precision digits. The

reason that the contours are jagged is because the code set is discrete, and therefore, the system is unable to find the real number optimal rate, but rather chooses the closest available code rate. Clearly, as the packet size decreases, the performance improvement increases because the PER decreases. However, the PSNR performances of all the compared systems become lower because of the increased overhead and redundancy introduced by the CRC and channel coding. For example, when  $\nu \approx 200$  and  $r_{\text{tr}} \approx 1$ ,  $\Delta\text{PSNR} \approx 4.27$  dB, yet the EEP system has  $\text{PSNR} = 25.5$  dB, which is very low quality, and the UEP due only to packetization has  $\text{PSNR} = 30$  dB, which is significantly better, but still not high quality. In addition, at small enough packet sizes, the performance improvement is small because  $N$  becomes large, and both systems use the same optimal channel code rate. In addition, the performance improvement increases with the transmission rate for the range of rates considered.

### F. Computational Complexity

We experimentally observed the following. For a fixed  $\mathbf{r}$ , bit budget constraint  $B$ , and packet size  $\nu$ , the computational complexity of the optimization procedure [i.e., solving (10)] grows approximately linearly with the number of optimized hierarchical parameters ( $|\alpha|$ ). Note that the most complex optimization procedure belongs to foldHier2. After running an exhaustive search for the best code rate, the complexity of the optimization procedure for foldHier2 grows at most quadratically in the number of elements in  $C_r$  and linearly in the number of hierarchical parameters (and therefore in the number of packets). The growth is at most quadratic because, for some code rates, the numerical optimization tools we use terminate early in their iterations simply because those code rates are either too weak or too powerful for a given channel state.

## V. PROPOSED SCHEME UNDER FREQUENCY-SELECTIVE CHANNELS

In this section, we will extend our results from AWGN and flat Rayleigh fading channels to frequency-selective channels. We consider a single carrier system for transmitting a progressive bit stream through a frequency-selective channel. We use equalization to combat the ISI due to the frequency selectivity of the channel. We will show that for this channel, the combining/packetization strategy yields performance improvement compared with other UEP schemes and the EEP scheme introduced in the previous section.

We consider short-distance high-data-rate communications, where the line of sight (LOS) component of the channel can be lost through random link breaks. Examples include wireless Internet connections in malls, airports, and hotels. In capacious spaces such as these, the multipath delay spread is large, so the coherence bandwidth is fairly small. At reasonably high data rates, the required bandwidth would typically exceed the coherence bandwidth, and the channel will be characterized as being frequency selective. The random link breaks are commonly due to mobile objects obstructing the transmitter–receiver direct communication. In malls, airports, and hotels, link breakages are common because of people walking around. Therefore,

we are interested in considering such scenarios involving both frequency-selective channels and link breaks.

The symbol duration is assumed to be small enough that the fading coefficients are constant during the transmission of a symbol. Since the cost function is difficult to formulate in closed form, and exhaustive search is not a plausible option, it is infeasible to optimize all the parameters of the system for the given frequency-selective channel. Instead, we use the optimized hierarchical parameters found for a flat Rayleigh fading case at a given average SNR and then optimize the channel code rates. In other words, an optimal rate schedule is found based on a suboptimal hierarchical parameter set for the given channel model. The performance results will be shown to give gains of around 1 dB over the EEP scheme and can be thought of as lower bounds on the performance improvement of the fully optimized system over the EEP scheme.

### A. Channel Model

In multipath channels, paths often arrive in clusters. Our channel model includes this clustering phenomenon and random fading gains with deterministic multipath delays, very similar to the clustering phenomenon found in IEEE 802.15.3c [35]. The first tap gain of the channel is given as a mixture of Rician and Rayleigh distributions to model an abrupt link breakage. The parameter  $\kappa$  is used to denote the percentage of time that the LOS link is available. Non-LOS (NLOS) components are Rayleigh distributed.

The general fading process is a two-component complex stationary random process for the  $i$ th multipath, which is described as  $h_i(t) = \delta_{i,0}\Gamma_i(t)e^{j\Psi_i(t)} + \tilde{a}_i(t)$ ,  $i = 0, 1, \dots$  [35], where  $\Gamma_i(t)$  is the amplitude of the specular component of the  $i$ th multipath of the fading process,  $\Psi_i(t)$  is the uniformly distributed random phase of the specular component of the  $i$ th multipath, and  $\tilde{a}_i(t)$  is the diffuse fading component of the  $i$ th multipath, which is usually assumed to be a complex zero-mean Gaussian process with independent in-phase and quadrature components, each with variance  $\sigma_{a_i}^2$ . We drop the time dependence hereafter because the channel coefficients are assumed to be the same during the transmission of any particular symbol. However, the channel coefficients are allowed to vary from one symbol to another. The current LOS component is statistically dependent on the previous state of the LOS component of the channel. We assume that when there is no LOS component ( $\Gamma_0 = 0$ ), the probability of having an LOS component in the next transmission is  $p_1$ . Similarly, when there is an LOS component ( $\Gamma_0 \neq 0$ ), the probability of having no LOS component in the next transmission is  $p_2$ .

For the first subpath, we have a Rician distribution, conditioned on  $\Gamma_0$ , given by  $f_R(r|\Gamma_0) = (r/\sigma_{a_0}^2) \exp\{-(r^2 + \Gamma_0^2)/2\sigma_{a_0}^2\} I_0(r\Gamma_0/\sigma_{a_0}^2)$ , where  $I_0(\cdot)$  is the modified Bessel function of the first kind with order zero. In addition, for other NLOS components ( $\Gamma_j = 0$ ,  $j = 1, 2, \dots$ ), the Rayleigh distribution for the  $i$ th multipath ( $i = 1, \dots$ ) is given by  $f_x(x) = (x/\sigma_{a_i}^2) \exp\{-(x^2/2\sigma_{a_i}^2)\}$ . The ratio of specular-to-diffuse energy of the first subpath fading component is defined to be ( $K$ -factor)  $K = \Gamma_0^2/2\sigma_{a_0}^2$  and is usually expressed in decibels. Since an AWGN channel has a tap gain with power unity,

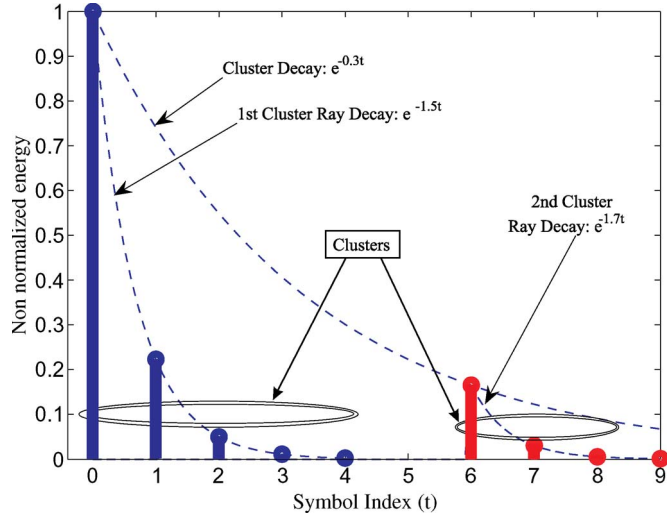


Fig. 14. Sample energy decay profile.

we choose the same power constraint on this channel, i.e.,  $\mathbb{E}[\sum_i |h_i|^2] = \sum_i \mathbb{E}[|h_i|^2] = 1$ , where  $\mathbb{E}[\cdot]$  denotes the ensemble average [28].

Our frequency-selective channel is assumed to consist of  $M$  complex channel coefficients  $\mathbf{h} = [h_0, h_1, \dots, h_{M-1}]$ . Let  $\phi_i = E[|h_i|^2] = \delta_{i,0} \Gamma_i^2 + 2\sigma_{a_i}^2 \in \mathbb{R}$  be the power coefficient for each subpath. Thus, the power vector is given by  $\phi = [\phi_0, \phi_1, \dots, \phi_{M-1}]$ , the entries of which satisfy the power constraint. We use a simplified discrete-time domain representation for the impulse response of the channel. The time axis is divided into  $M$  equal time intervals, i.e., each single multipath component is separated by an integer multiple of  $1/B$  compared with other multipaths such that  $M/B \geq \sigma_T$ , where  $\sigma_T$  is the root mean square delay spread of the channel, and  $B$  is the bandwidth of the baseband equivalent signal. Thus, we write the impulse response as follows:

$$\Theta(\tau) = \sum_{i=0}^{M-1} h_i \delta(\tau - i/B). \quad (19)$$

Typical values for the channel parameters can be found in various specifications for channel models, such as COST 207 [36] or Stanford University Interim [37]. In our model, similar to [35] and [36], we assume exponential decay of multipath energy. In modeling it, we assume two clusters, each having their own decay rate, where the cluster decay is modeled using an exponential function. One sample profile based on [36] is shown in Fig. 14, where each subpath is placed at the beginning of each subinterval. The multipath delay spread is assumed to be  $9/B$  for this particular case. Finally, the parameter  $\kappa$  represents the percentage of time that the LOS component is available. Since we have a two-state Markov chain, it can be shown that  $\kappa = (p_1/(p_2 + p_1)) \times 100$ .

### B. Numerical Results for a Frequency-Selective Channel

We use a nine-tap equalizer at the receiver based on the minimum MSE (MMSE) criterion to mitigate the effects of ISI on the overall system performance. We assume perfect CSI at the receiver, i.e., the channel tap gains are known at the receiver.

TABLE I  
SIMULATION PARAMETERS ( $T$ : SYMBOL DURATION)

Channel Parameters			
Parameter name	$\mathbf{h}_1$	$\mathbf{h}_2$	$\mathbf{h}_3$
Cluster decay	$e^{-0.74t}$	$e^{-0.72t}$	$e^{-0.53t}$
1st Cluster Ray decay	$e^{-6.81t}$	$e^{-2.65t}$	$e^{-1.77t}$
2nd Cluster Ray decay	$e^{-2.51t}$	$e^{-1.89t}$	$e^{-0.81t}$
$\kappa$	71%	71%	71%
$M$	8	7	7
$\sigma_T$	$0.5878T$	$0.6626T$	$1.3459T$
$p_1$	0.81	0.81	0.81/1
$p_2$	0.33	0.33	0.33/0
Coherence time	$9T$	$9T$	$9T$
$K$ (in dB)	10	10	10

The channel tap coefficients stay the same during a duration of nine symbols ( $9T$ , where  $T$  is the symbol duration) and then change based on their corresponding energy decay profiles. A summary of simulation parameters (parameter values of ((19))) for each frequency-selective channel is given in Table I.

Based on the estimated channel tap gains and the current average SNR ( $= E_b/N_o E[|h_o^2|]$ ), the MMSE equalizer taps are calculated for each nine-symbol transmission period and used to equalize the system. Note that when the channel state changes, the corresponding equalizer tap coefficients are re-computed immediately according to the new channel state. We tested three sample channels with the following power decay profiles [36]:

$$\phi_1 = [0.986, 0.0011, 0, 0, 0, 0.012, 0, 0.001] \quad (20)$$

$$\phi_2 = [0.921, 0.065, 0, 0, 0, 0.0117, 0.0018, 0] \quad (21)$$

$$\phi_3 = [0.78, 0.125, 0.047, 0, 0, 0.0321, 0.0164, 0]. \quad (22)$$

In what follows, we show some simulation results using RCPC channel codes in conjunction with H-16QAM and folded packetization for three different channels. We vary  $E_b/N_o$  to obtain different values of the average SNR, as shown in the abscissa of each plot. First, in Fig. 15, the decoded BER performance as a function of average SNR is shown for channels  $\mathbf{h}_1$ ,  $\mathbf{h}_2$ , and  $\mathbf{h}_3$ , with and without MMSE equalization, using channel parameters  $p_1 = 0.81$ ,  $p_2 = 0.33$ , and  $K = 10$  dB, which is equivalent to  $\kappa = 71\%$  LOS availability. The simulations are run using the optimal code rates that minimize the average distortion of seqConv1, as shown in the title of each plot. As can be seen, the equalization improves the system performance by lowering the HP and LP BERs while preserving the BER gap in between.

Next, we show some of the results of an image transmission ( $512 \times 512$  grayscale Lena image encoded with SPIHT) using the channel  $\mathbf{h}_3$ , and compare different packetizations using H-16QAM at an average received SNR  $\sim 13.9$  dB and transmission rate  $r_{tr} = 0.25$  bpp. For better understanding of the performance, we plot the cumulative distribution function (cdf) of the PSNR. We also show the average PSNR values in parentheses.

Since it is infeasible to optimize the hierarchical parameters of the systems foldHier1 and foldHier2 for the given frequency-selective channel, we use the optimal hierarchical parameter values found for the flat Rayleigh fading case. Fig. 16 compares

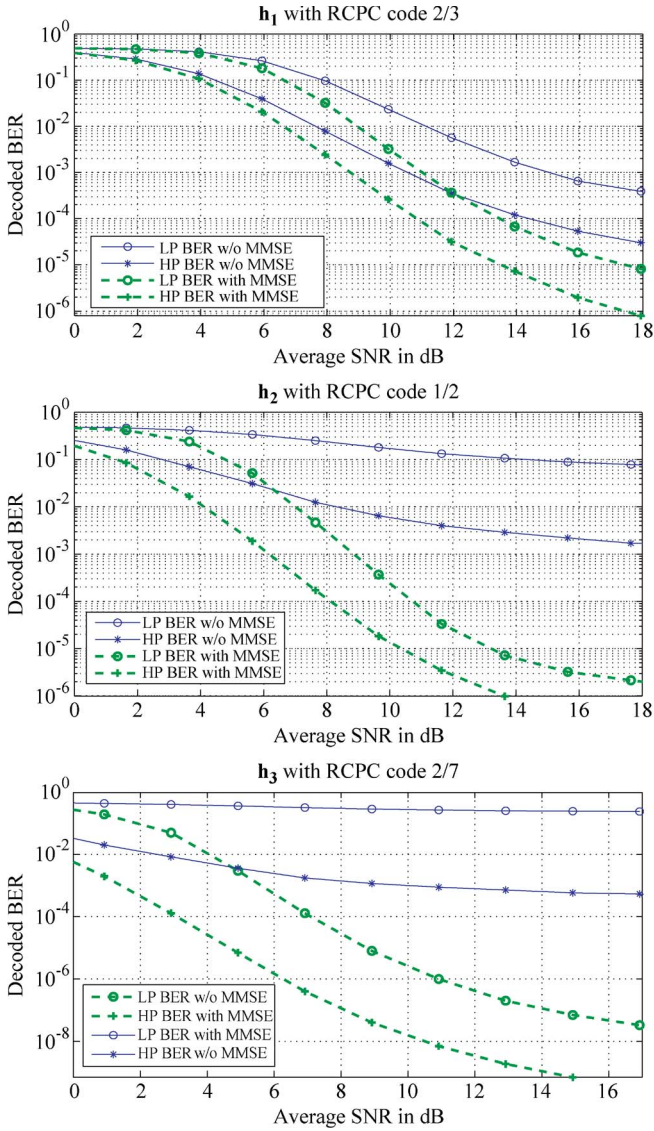


Fig. 15. Effect of the equalization for various frequency-selective channels  $h_1$ ,  $h_2$ , and  $h_3$ .

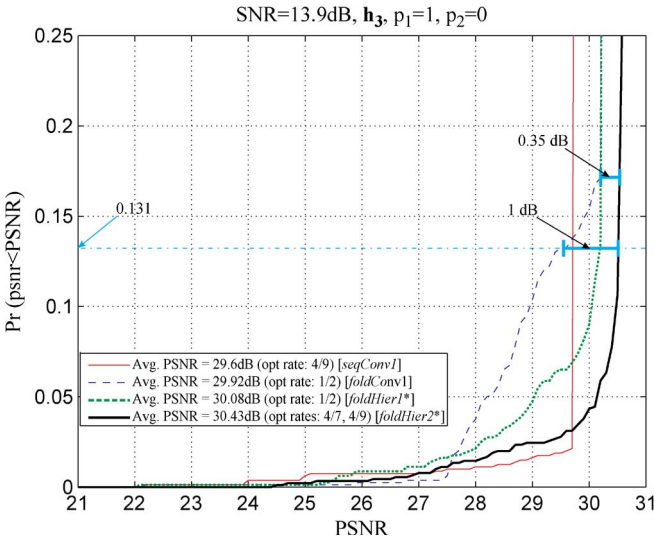


Fig. 16. CDF of PSNR for the frequency-selective channel  $h_3$  without link breakage, as the UEP is more effective with degrading channel conditions.

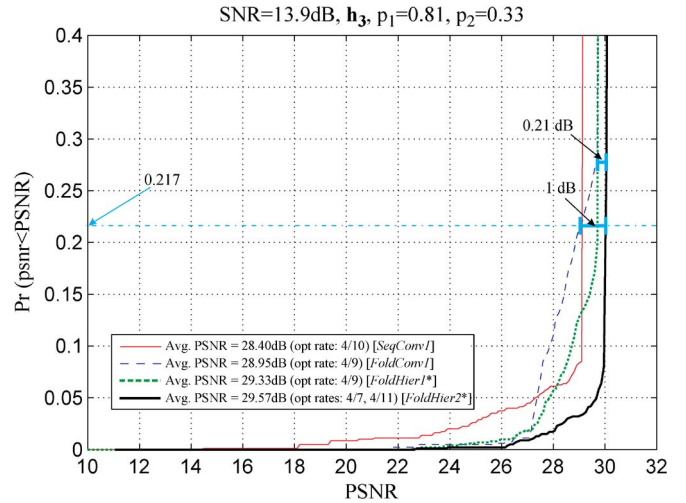


Fig. 17. CDF of PSNR for the frequency-selective channel  $h_3$  without link breakage using equalization.

the cdf of PSNR performances of the optimal seqConv1 and foldConv1 and the suboptimal foldHier1 (foldHier1\*) and foldHier2 (foldHier2\*) systems under the no link breakage assumption, i.e.,  $p_1 = 1$ ,  $p_2 = 0$ . The figure suggests that by simply switching the packetization scheme, i.e., going from seqConv1 to foldConv1, we pick up around 0.3-dB gain in average PSNR. When we use suboptimal hierarchical parameters with a single optimal code rate (foldHier1\*), we pick up an additional 0.2 dB in average PSNR over foldConv1. Finally, foldHier2\* gives more than 0.35-dB average PSNR improvement over foldHier1\*. In total, foldHier2\* improves the average PSNR performance upon EEP by more than 0.85 dB. Another observation is that foldHier2\* gives more than 1-dB PSNR improvement over foldConv1 around 13% of the time.

In Fig. 17, we consider the link breakage by setting  $p_1 = 0.81$  and  $p_2 = 0.33$ . When we optimize the system foldHier1 for a flat Rayleigh fading channel, the optimal code rate turns out to be 4/9. Let us denote the corresponding optimal hierarchical parameter vector as  $\alpha_{4/9}^*$ . If we use the optimal code rate in conjunction with  $\alpha_{4/9}^*$  under our frequency-selective channel model, then foldHier1\* gives an average PSNR of 29.33 dB. When we use optimal double code rates (one for the first half and one for the second half of the bit stream), i.e., the optimal code rate schedule ( $\mathbf{r}^*$ ) using  $\alpha_{4/9}^*$  for the given frequency-selective channel, the optimal channel code rates turn out to be (4/7, 4/11), and the average PSNR is 29.57 dB. As can be seen using the channel  $h_3$ , the partially optimized system foldHier2\* still gives around 1-dB average PSNR performance improvement over the EEP scheme seqConv1, which is around the same gain seen in flat-fading cases. Therefore, one can expect more than 1-dB average PSNR gain over the EEP by jointly optimizing the code rates and hierarchical parameters (foldHier2). In addition, foldHier2\* gives more than 1-dB PSNR improvement over foldConv1 around 21% of the time. Comparing this with the no-link break scenario (13% of the time), the proposed scheme is more effective with growing probability of link breakage using equalization.

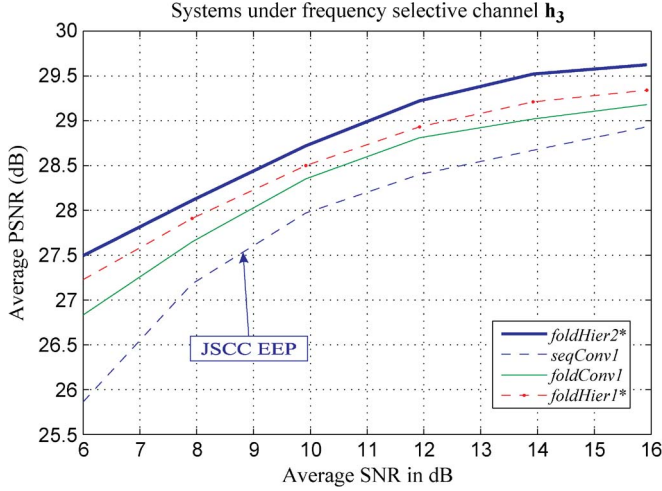


Fig. 18. Performance of different systems for a frequency-selective channel with link breaks using  $\mathbf{h}_3$  and  $p_1 = 0.81$  and  $p_2 = 0.33$ . JSSC EEP is also shown for comparison. The results correspond to the *Lena* image.

Finally, Fig. 18 shows PSNR versus average SNR performance of various systems using the *Lena* image and the frequency-selective channel  $\mathbf{h}_3$  with  $p_1 = 0.81$  and  $p_2 = 0.33$ . Similar gains are observed for a range of average SNR values.

## VI. CONCLUSION

In this paper, we have presented a reliable and robust progressive source encoding scheme for fixed packet length image transmission based upon the combined use of several UEP methods. Several different transmission channels are assumed: AWGN, independent flat fading channels, and a frequency-selective channel that accounts for link breakage. Specifically, a packetization methodology that is coupled with both hierarchical modulation and FEC is considered. It is shown in this study that the different UEP methods can judiciously be combined to provide enhanced reliability for the transmission of the progressive source, as one of the methods usually alleviates the constraints coming from the others. A lower bound for the performance improvement of the proposed system is derived and shown for various packet sizes and transmission rates to be an indicator for usefulness of the proposed system.

## APPENDIX

### LOWER BOUND ON THE PERFORMANCE IMPROVEMENT OF THE PROPOSED SYSTEM

Let us denote the total distortion measure  $\mathfrak{D}_N^j(\alpha; \mathcal{A})$  using only the packets in set  $\mathcal{A}$  and packetization  $j \in \{SP, FP\}$  in an  $N$ -packet error protection scheme. Note that from (9) and previous discussion, we have  $\mathbb{E}[\mathfrak{D}^{SP}(R^*, R^*, \alpha_3)] := d_0 + \mathfrak{D}_N^{SP}(\alpha_3; \Omega)$  and  $\mathbb{E}[\mathfrak{D}^{FP}(R^*, R^*, \alpha_3)] := d_0 + \mathfrak{D}_N^{FP}(\alpha_3; \Omega)$ .

Let  $p_{HP}$  and  $p_{LP}$  be the probability of having HP and LP packets correct, using  $R^*$  and  $\alpha_3$ . The PER gap is defined as  $p_{HP} - p_{LP} \triangleq \Delta\gamma$ . It can be shown by induction that  $(p_{HP})^n - (p_{LP})^n = \Delta\gamma\phi_{n-1}$ , where  $\phi_n$  satisfies the recursive relation  $\phi_n = p_{HP}\phi_{n-1} + (p_{LP})^n$  with the initial condition  $\phi_0 = 1$ . Note also that  $\forall n \in \mathbb{N}$ ,  $\phi_n \geq 0$ , and we define  $\phi_n = 0$  for  $n < 0$ .

We will show that  $\mathbb{E}[\mathfrak{D}^{SP}(R^*, R^*, \alpha_3)] - \mathbb{E}[\mathfrak{D}^{FP}(R^*, R^*, \alpha_3)] = \mathfrak{D}_N^{SP}(\alpha_3; \Omega) - \mathfrak{D}_N^{FP}(\alpha_3; \Omega) \geq 0$ . Let us find the total distortion measure gap in the first half as follows (i.e., bits in  $\mathcal{P}'_U$ ):

$$\begin{aligned} \Delta\mathfrak{D}_N(\mathcal{P}'_U) &\triangleq \mathfrak{D}_N^{SP}(\alpha_3; \mathcal{P}'_U) - \mathfrak{D}_N^{FP}(\alpha_3; \mathcal{P}'_U) \\ &= -\sum_{l=1}^{N/2} \prod_{i=1}^l P_i^{(SP)} \Delta_l - \left( -\sum_{l=1}^{N/2} \prod_{i=1}^l P_i^{(FP)} \Delta_l \right) \end{aligned} \quad (23)$$

where the probability of having packet  $i$  correct for the system using  $FP$ ,  $P_i^{(FP)} = p_{HP}$ , for  $1 \leq i \leq N/2$ ,  $P_i^{(FP)} = p_{LP}$  for  $(N/2) + 1 \leq i \leq N$ . In addition, for the system using  $SP$  and from Fig. 3(b), we have  $P_i^{(SP)} = p_{HP}$  if  $i$  is odd and  $P_i^{(SP)} = p_{LP}$  if  $i$  is even. Similarly, the total distortion measure gap in the second half (i.e., bits in  $\mathcal{P}''_U$ ) is given by

$$\begin{aligned} \Delta\mathfrak{D}_N(\mathcal{P}''_U) &\triangleq \mathfrak{D}_N^{SP}(\alpha_3; \mathcal{P}''_U) - \mathfrak{D}_N^{FP}(\alpha_3; \mathcal{P}''_U) \\ &= -\sum_{l=\frac{N}{2}+1}^N \prod_{i=1}^l P_i^{(SP)} \Delta_l + \sum_{l=\frac{N}{2}+1}^N \prod_{i=1}^l P_i^{(FP)} \Delta_l. \end{aligned} \quad (24)$$

### A. $N$ Is Divisible by Four

First, assume that  $N$  is divisible by 4. We have

$$\begin{aligned} \Delta\mathfrak{D}_N(\mathcal{P}'_U) &= p_{HP}\Delta_1 - p_{HP}\Delta_1 + p_{HP}^2\Delta_2 - p_{HP}p_{LP}\Delta_2 \dots \\ &\quad + p_{HP}^{\frac{N}{2}}\Delta_{N/2} - p_{HP}^{\frac{N}{4}}p_{LP}^{\frac{N}{4}}\Delta_{N/2} \\ &= 0 + p_{HP}(p_{HP} - p_{LP})\Delta_2 + \dots \end{aligned} \quad (25)$$

$$+ p_{HP}^{\frac{N}{4}} \left( p_{HP}^{\frac{N}{4}} - p_{LP}^{\frac{N}{4}} \right) \Delta_{N/2} \quad (26)$$

$$= \sum_{n=1}^{\frac{N}{4}} p_{HP}^n \Delta\gamma(\phi_{n-2}\Delta_{2n-1} + \phi_{n-1}\Delta_{2n}). \quad (27)$$

Let us consider the second half:

$$\Delta\mathfrak{D}_N(\mathcal{P}''_U) \quad (28)$$

$$= +p_{HP}^{\frac{N}{2}} p_{LP} \Delta_{\frac{N}{2}+1} + \dots + p_{HP}^{\frac{N}{2}} p_{LP}^{\frac{N}{2}} \Delta_N \quad (29)$$

$$- p_{HP}^{\frac{N}{4}+1} p_{LP}^{\frac{N}{4}} \Delta_{\frac{N}{2}+1} - \dots - p_{HP}^{\frac{N}{2}} p_{LP}^{\frac{N}{2}} \Delta_N$$

$$= p_{HP}^{\frac{N}{4}+1} p_{LP} \left( p_{HP}^{\frac{N}{4}-1} - p_{LP}^{\frac{N}{4}-1} \right) \Delta_{\frac{N}{2}+1} \quad (30)$$

$$+ p_{HP}^{\frac{N}{4}+1} p_{LP}^2 \left( p_{HP}^{\frac{N}{4}-1} - p_{LP}^{\frac{N}{4}-1} \right) \Delta_{\frac{N}{2}+2} \dots \quad (31)$$

$$= \sum_{n=1}^{\frac{N}{4}} p_{HP}^{\frac{N}{4}+n} p_{LP}^{2n-1} \Delta\gamma\phi_{\frac{N}{4}-n-1} \left( \Delta_{\frac{N}{2}+2n-1} + p_{LP} \Delta_{\frac{N}{2}+2n} \right). \quad (32)$$

Therefore, since  $\mathcal{P}'_U \cap \mathcal{P}''_U = \emptyset$  and  $\mathfrak{D}_N^j(\alpha_3; \cdot)$  is a finitely additive measure, we obtain

$$\begin{aligned} \mathbb{E}[\mathfrak{D}^{SP}(R^*, R^*, \alpha_3)] - \mathbb{E}[\mathfrak{D}^{FP}(R^*, R^*, \alpha_3)] \\ &:= \Delta\mathfrak{D}_N(\Omega) = \mathfrak{D}_N^{SP}(\Omega) - \mathfrak{D}_N^{FP}(\Omega) \\ &= \mathfrak{D}_N^{SP}(\mathcal{P}'_U) + \mathfrak{D}_N^{SP}(\mathcal{P}''_U) - \mathfrak{D}_N^{FP}(\mathcal{P}'_U) - \mathfrak{D}_N^{FP}(\mathcal{P}''_U) \\ &= \Delta\mathfrak{D}_N(\mathcal{P}'_U) + \Delta\mathfrak{D}_N(\mathcal{P}''_U) \\ &= \sum_{n=1}^{\frac{N}{4}} p_{HP}^n \Delta\gamma[\phi_{n-2}\Delta_{2n-1} + \phi_{n-1}\Delta_{2n}] \end{aligned}$$

$$\begin{aligned}
& + \sum_{n=1}^{\frac{N}{4}} p_{\text{HP}}^{\frac{N}{4}+n} p_{\text{LP}}^{2n-1} \Delta \gamma \phi_{\frac{N}{4}-n-1} \left( \Delta_{\frac{N}{2}+2n-1} + p_{\text{LP}} \Delta_{\frac{N}{2}+2n} \right) \\
& = \sum_{n=1}^{\frac{N}{4}} p_{\text{HP}}^n \Delta \gamma \left( \phi_{n-2} \Delta_{2n-1} + \phi_{n-1} \Delta_{2n} + p_{\text{HP}}^{\frac{N}{4}} p_{\text{LP}}^{2n-1} \right. \\
& \quad \left. \times \phi_{\frac{N}{4}-n-1} \left( \Delta_{\frac{N}{2}+2n-1} + p_{\text{LP}} \Delta_{\frac{N}{2}+2n} \right) \right) \\
& \geq 0. \tag{33}
\end{aligned}$$

### B. $N$ Is Not Divisible by 4

When  $N$  is not divisible by 4, a similar derivation will follow except (27) and (32) will be given by

$$\begin{aligned}
\Delta \mathcal{D}_N(\mathcal{P}'_{\cup}) & = \sum_{n=1}^{\frac{N-2}{4}} p_{\text{HP}}^n \Delta \gamma [\phi_{n-2} \Delta_{2n-1} + \phi_{n-1} \Delta_{2n}] \\
& \quad + p_{\text{HP}}^{\frac{N+2}{4}} \Delta \phi_{\frac{N-2}{4}-1} \Delta_{N/2} \\
\Delta \mathcal{D}_N(\mathcal{P}''_{\cup}) & = \sum_{n=1}^{\frac{N-2}{4}} p_{\text{HP}}^{\frac{N+2}{4}+n} p_{\text{LP}}^{2n} \Delta \gamma \phi_{\frac{N-2}{4}-n-1} \\
& \quad \times \left( \Delta_{\frac{N}{2}+2n} + p_{\text{LP}} \Delta_{\frac{N}{2}+2n+1} \right) \\
& \quad + p_{\text{HP}}^{\frac{N+2}{4}} p_{\text{LP}} \Delta \gamma \phi_{\frac{N-2}{4}-1} \Delta_{\frac{N}{2}+1}.
\end{aligned}$$

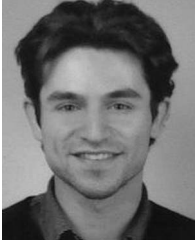
Thus,  $\Delta \mathcal{D}_N(\mathcal{P}'_{\cup}) + \Delta \mathcal{D}_N(\mathcal{P}''_{\cup}) \geq 0$ , since  $\{\Delta_l\}_{l=1}^N \geq 0$ . ■

### ACKNOWLEDGMENT

The authors would like to thank various anonymous reviewers for their valuable comments and suggestions.

### REFERENCES

- [1] N. Matoba and S. Yoshida, "Still image transmission using unequal error protection coding in mobile radio channel," *Electron. Commun. Jpn.*, vol. 79, no. 4, pp. 75–85, 1996.
- [2] J. Lu, A. Nosratinia, and B. Aazhang, "Progressive source channel coding of images over bursty error channels," in *Proc. Int. Conf. Image Process.*, Chicago, IL, Oct. 1998, pp. 127–131.
- [3] P. G. Sherwood and K. Zeger, "Progressive image coding for noisy channels," *IEEE Signal Process. Lett.*, vol. 4, no. 7, pp. 189–191, Jul. 1997.
- [4] T. Thomos, N. V. Boulgouris, and M. G. Strintzis, "Wireless image transmission using turbo codes and optimal unequal error protection," *IEEE Trans. Image Process.*, vol. 14, no. 11, pp. 1890–1901, Nov. 2005.
- [5] X. Pan, A. H. Banihashemi, and A. Cuhadar, "Progressive transmission of images over fading channels using rate-compatible LDPC codes," *IEEE Trans. Image Process.*, vol. 15, no. 12, pp. 3627–3635, Dec. 2005.
- [6] L. Li and M. Salehi, "Hierarchical image coding matched to unequal error protection rate compatible punctured convolutional codes," in *Proc. IEEE Int. Conf. Robot., Intell. Syst. Signal Process.*, Oct. 2003, vol. 1, pp. 238–243.
- [7] A. Said and W. A. Pearlman, "A new fast and efficient image codec based on set partitioning in hierarchical trees," *IEEE Trans. Circuits Syst. Video Technol.*, vol. 6, no. 3, pp. 243–250, Jun. 1996.
- [8] M. Sajadieh, F. Kschischang, and A. Leon-Garcia, "Modulation-assisted unequal error protection over the fading channel," *IEEE Trans. Veh. Technol.*, vol. 47, no. 3, pp. 900–908, Aug. 1998.
- [9] P. Ma and K. S. Kwak, "Modulation-assisted UEP-LDPC codes in image transmission," in *Proc. IEEE ISCIT*, 2009, pp. 230–233.
- [10] J. Song and K. J. R. Liu, "Robust progressive image transmission over OFDM systems using space-time block code," *IEEE Trans. Multimedia*, vol. 4, no. 3, pp. 394–406, Sep. 2002.
- [11] Y. Sun and Z. Xiong, "Progressive image transmission over space-time coded OFDM-based MIMO systems with adaptive modulation," *IEEE Trans. Mobile Comput.*, vol. 4, no. 8, pp. 1016–1028, Aug. 2006.
- [12] *Digital Video Broadcasting (DVB); Framing Structure, Channel Coding and Modulation for Digital Terrestrial Television*, ETSI, EN 300 744, V1.5.1, Nov. 2004.
- [13] C.-E. W. Sundberg, W. C. Wong, and R. Steele, "Logarithmic PCM weighted QAM transmission over Gaussian and Rayleigh fading channels," *Proc. Inst. Elect. Eng.—F*, vol. 134, no. 6, pp. 557–570, Oct. 1987.
- [14] M. Morimoto, M. Okada, and S. Komaki, "A hierarchical image transmission system for multimedia mobile communication," in *Proc. 1st Int. Workshop Wireless Image/Video Commun.*, Sep. 1996, pp. 80–84.
- [15] S. O'Leary, "Hierarchical transmission and COFDM systems," *IEEE Trans. Broadcast.*, vol. 43, no. 2, pp. 166–174, Jun. 1997.
- [16] H. X. Nguyen, H. H. Nguyen, and T. Le-Ngoc, "Signal transmission with unequal error protection in wireless relay networks," *IEEE Trans. Veh. Technol.*, vol. 59, no. 5, pp. 2166–2178, Jun. 2010.
- [17] J. E. Kleider and G. P. Aousleman, "Robust image transmission using source adaptive modulation and trellis-coded quantization," in *Proc. ICIP*, 1999, vol. 1, pp. 396–400.
- [18] Y. Pei and J. W. Modestino, "Multi-layered video transmission over wireless channels using an adaptive modulation and coding scheme," in *Proc. IEEE Int. Conf. Image Process.*, Oct. 2001, vol. 2, pp. 1009–1012.
- [19] M. Ghandi, B. Barmada, E. Jones, and M. Ghanbari, "Unequally error protected data partitioned video with combined hierarchical modulation and channel coding," in *Proc. IEEE Int. Conf. Acoust., Speech, Signal Process.*, May 2006, vol. 2, pp. II-529–II-532.
- [20] J. Hagenauer, "Rate-compatible punctured convolutional (RCPC) codes and their applications," *IEEE Trans. Commun.*, vol. 36, no. 4, pp. 389–400, Apr. 1988.
- [21] H. Dubois-Ferriere, D. Estrin, and M. Vetterli, "Packet combining in sensor networks," in *Proc. 3rd Int. Conf. Embedded Netw. Sens. Syst.*, San Diego, CA, Nov. 2005, pp. 102–115.
- [22] S. S. Chakraborty, "An ARQ scheme with packet combining," *IEEE Commun. Lett.*, vol. 2, no. 7, pp. 200–202, Jul. 1995.
- [23] T. C. Bhunia, "Packet reversed packet combining scheme," in *Proc. 7th IEEE Int. Conf. CIT*, 2007, pp. 447–451.
- [24] S. H. Chang, M. Rim, P. C. Cosman, and L. B. Milstein, "Optimized unequal error protection using multiplexed hierarchical modulation," in *IEEE Trans. Inf. Theory*, to be published.
- [25] S. S. Arslan, P. C. Cosman, and L. B. Milstein, "Progressive source transmissions using joint source-channel coding and hierarchical modulation in packetized networks," in *Proc. IEEE GLOBECOM*, 2009, pp. 1–6.
- [26] P. K. Vitthaladevuni and M.-S. Alouini, "BER computation of 4/M-QAM hierarchical constellations," *IEEE Trans. Broadcast.*, vol. 47, no. 3, pp. 228–239, Sep. 2001.
- [27] S. S. Arslan, P. C. Cosman, and L. B. Milstein, "On hard decision upper bounds for coded m-ary hierarchical modulation," in *Proc. IEEE CISS*, Baltimore, MD, 2011, pp. 1–6.
- [28] J. G. Proakis, *Digital Communications*, 3rd ed. New York: McGraw-Hill, 1995.
- [29] D. J. Costello and O. Y. Takeshita, "On the packet error rate of convolutional codes," in *Proc. Inf. Theory Netw. Workshop*, Jun. 1999, p. 29.
- [30] L. Cao, "On the unequal error protection for progressive image transmission," *IEEE Trans. Image Process.*, vol. 16, no. 9, pp. 2384–2388, Sep. 2007.
- [31] S. Boyd and L. Vandenberg, *Convex Optimization*. Cambridge, U.K.: Cambridge Univ. Press, 2004.
- [32] J. A. Snyman, *Practical Mathematical Optimization: An Introduction to Basic Optimization Theory and Classical and New Gradient-Based Algorithms*. New York: Springer-Verlag, 2005.
- [33] H. Yousefzadeh, H. Jafarkhani, and F. Etemadi, "Distortion-optimal transmission of progressive images over channels with random bit errors and packet erasures," in *Proc. IEEE DCC*, 2004, pp. 132–141.
- [34] A. Skodras, C. Christopoulos, and T. Ebrahimi, "The JPEG2000 still image compression standard," *IEEE Signal Process. Mag.*, vol. 18, no. 5, pp. 36–58, Sep. 2001.
- [35] *IEEE 802.15 WPAN Millimeter Wave Alternative PHY Task Group 3c*, IEEE 802.15.3c-2009, 2009.
- [36] "COST 207: Digital land mobile radio communications," Office Official Publ. Eur. Commun., Luxembourg City, Luxembourg, Final Rep., 1989.
- [37] K. V. S. Hari, D. S. Baum, and P. Soma, "Channel models for fixed wireless applications," IEEE 802.16 Broadband Wireless Access Working Group, 2003.



**Suayb S. Arslan** (S'06) received the B.S. degree in electrical and electronics engineering in 2006 from Bogazici University, Istanbul, Turkey, and the M.S. degree in electrical and computer engineering in 2009 from the University of California, San Diego, La Jolla, where he is currently working toward the Ph.D. degree.

During the Summer of 2009, he was with Mitsubishi Electric Research Laboratory, Boston, MA, where he was involved in the research and development of image/video processing algorithms for biomedical applications. In the Summer of 2011, he joined Quantum Corporation, Irvine, CA, where he conducted research on advanced detection algorithms and postprocessing for increased capacity tape drives. He is currently with the Department of Electrical and Computer Engineering, University of California, San Diego. His research interests include wireless/wireline digital multimedia communications, joint source channel coding, information theory, image/video processing, and cross-layer design optimizations.

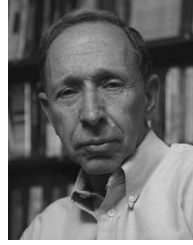


**Pamela C. Cosman** (S'88–M'93–SM'00–F'08) received the B.S. degree (hons) in electrical engineering from the California Institute of Technology, Pasadena, in 1987 and the M.S. and Ph.D. degrees in electrical engineering from Stanford University, Stanford, CA, in 1989 and 1993, respectively.

She was a National Science Foundation Postdoctoral Fellow with Stanford University and a Visiting Professor with the University of Minnesota, Minneapolis, during 1993–1995. In 1995, she joined the faculty of the Department of Electrical and Com-

puter Engineering, University of California, San Diego, La Jolla, where she is currently a Professor. She was the Director of the Center for Wireless Communications from 2006 to 2008. Her research interests are in the areas of image and video compression and processing and wireless communications.

Dr. Cosman is a member of Tau Beta Pi and Sigma Xi. She was a Guest Editor of the June 2000 special issue of the *IEEE JOURNAL ON SELECTED AREAS IN COMMUNICATIONS* on error-resilient image and video coding and the Technical Program Chair of the 1998 Information Theory Workshop in San Diego. She was an Associate Editor of the *IEEE COMMUNICATIONS LETTERS* (1998–2001) and an Associate Editor of the *IEEE SIGNAL PROCESSING LETTERS* (2001–2005). She was the Editor-in-Chief (2006–2009) as well as a Senior Editor (2003–2005, 2010–present) of the *IEEE JOURNAL ON SELECTED AREAS IN COMMUNICATIONS*. She was the recipient of the Electrical and Computer Engineering Departmental Graduate Teaching Award, a Career Award from the National Science Foundation, a Powell Faculty Fellowship, and a Globecom 2008 Best Paper Award.



**Laurence B. Milstein** (S'66–M'68–SM'77–F'85) received the B.E.E. degree from the City College of New York, in 1964 and the M.S. and Ph.D. degrees in electrical engineering from the Polytechnic Institute of Brooklyn, Brooklyn, NY, in 1966 and 1968, respectively.

From 1968 to 1974, he was with the Space and Communications Group, Hughes Aircraft Company, and from 1974 to 1976, he was a member of the Department of Electrical and Systems Engineering, Rensselaer Polytechnic Institute, Troy, NY. Since

1976, he has been with the Department of Electrical and Computer Engineering, University of California, San Diego (UCSD), La Jolla, where he is the Ericsson Professor of Wireless Communications Access Techniques and former Department Chairman, working in the area of digital communication theory with special emphasis on spread-spectrum communication systems. He has also been a Consultant to both government and industry in the areas of radar and communications.

Dr. Milstein was the Vice President for Technical Affairs in 1990 and 1991 of the IEEE Communications Society and is a former Chair of the IEEE Fellows Selection Committee. He was an Associate Editor for communication theory for the *IEEE TRANSACTIONS ON COMMUNICATIONS*, an Associate Editor for Book Reviews for the *IEEE TRANSACTIONS ON INFORMATION THEORY*, an Associate Technical Editor for the *IEEE Communications Magazine*, and the Editor-in-Chief of the *IEEE JOURNAL ON SELECTED AREAS IN COMMUNICATIONS*. He was the recipient of the 1998 Military Communications Conference Long-Term Technical Achievement Award, an Academic Senate 1999 UCSD Distinguished Teaching Award, an IEEE Third Millennium Medal in 2000, the 2000 IEEE Communication Society Armstrong Technical Achievement Award, and various prize paper awards, including the 2002 Military Communications Conference Fred Ellersick Award.